REPORT DOCUMENTATION PAGE

Form Approved OMB No. 0704-0188

1. AGENCY USE ONLY (Leave blank)	2. REPORT DATE	3. REPORT TYPE AND DATES COVERED
	27-July-2001	Final Report

4. TITLE AND SUBTITLE

Investigation Of An Alternative Geometry Hybrid Rocket For Small Spacecraft Orbit Transfer

5. FUNDING NUMBERS

F61775-00-WE036

6. AUTHOR(S)

Dave M Gibbon and Gary S Haag

7. PERFORMING ORGANIZATION NAME(S) AND ADDRESS(ES)

Surrey Satellite Technology, Ltd.
Surrey Space Center
University of Surrey
Guildford, Surrey GU2 5XH
United Kingdom

8. PERFORMING ORGANIZATION REPORT NUMBER

SPBB-26287-01

9. SPONSORING/MONITORING AGENCY NAME(S) AND ADDRESS(ES)

EOARD
PSC 802 BOX 14
FPO 09499-0200

10. SPONSORING/MONITORING AGENCY REPORT NUMBER

SPC 00-4036

11. SUPPLEMENTARY NOTES

12a. DISTRIBUTION/AVAILABILITY STATEMENT

Approved for public release; distribution is unlimited.

12b. DISTRIBUTION CODE

A

13. ABSTRACT (Maximum 200 words)

The following testing was carried out in support of the Surrey Space Centre (SSC) Alternative Geometry Hybrid Rocket research and development program. Although VFP testing was conducted in a low cost environment, the research program collected a wealth of valuable data with regard to this all-new hybrid rocket engine.

The combustion efficiency is outstanding within the VFP.

The scalability test has demonstrated that the VFP indeed scales well, providing high performance over the regimes tested as well as reliable, predictable, fuel liberation based upon the engine radius.

The chamber pressure mapping did not reveal any pressure gradient across the diameter of the VFP rocket engine over the regimes tested.

Flight propellant testing was promising in a number of areas.

The VFP has demonstrated the ability to operate smoothly for long durations (up to 45 seconds tested), and return to within 1.5% of operational values upon relight (pulsed operations). It is likely that the engine may be burned near completion without the fear of solid fuel slivers blocking the rocket nozzle. The VFP test campaign provides solid evidence that the VFP is superior to conventional hybrid design in almost every respect and holds great promise for small spacecraft applications.

14. SUBJECT TERMS	15. NUMBER OF PAGES
EOARD, Chemical Propulsion, Combustion, Rocket Engines, Vortex flows	47
	16. PRICE CODE: N/A

17. SECURITY CLASSIFICATION OF REPORT	18. SECURITY CLASSIFICATION OF THIS PAGE	19. SECURITY CLASSIFICATION OF ABSTRACT	20. LIMITATION OF ABSTRACT
UNCLASSIFIED	UNCLASSIFIED	UNCLASSIFIED	UL

SURREY
SATELLITE TECHNOLOGY LTD

Investigation of an Alternative Geometry Hybrid Rocket for Small Spacecraft Orbit Transfer

Dave Gibbon / Gary S. Haag

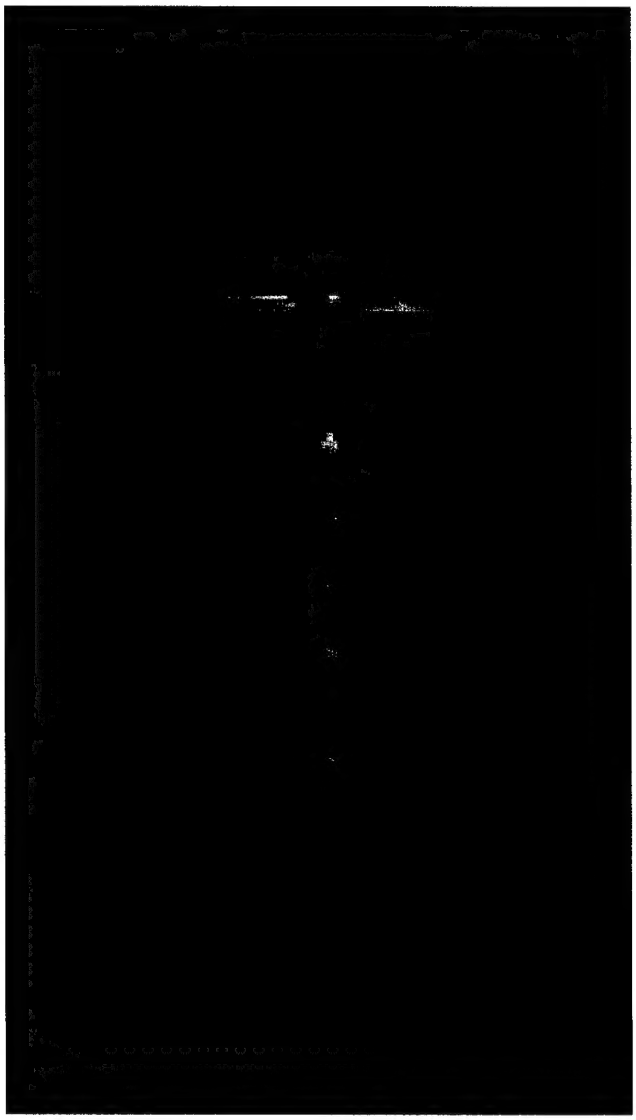

SPBB-26287-01

27 / July / 2001

Alternative Geometry Hybrid Rocket

01

Surrey Satellite Technology Limited,
Centre for Satellite Engineering Research,
University of Surrey,
Guildford,
Surrey,
GU2 5XH, UK
Tel: +44 1483 879817
Fax: +44 1483 879503
email: d.gibbon@eim..surrey.ac.uk

SURREY
SATELLITE TECHNOLOGY LTD

Investigation of an Alternative Geometry Hybrid Rocket for Small Spacecraft Orbit Transfer

Author(s)
Dave Gibbon / Gary S. Haag

Report No.
SPBB-26287-01

Date
27 / July / 2001

Subject
Alternative Geometry Hybrid Rocket

Revision
01

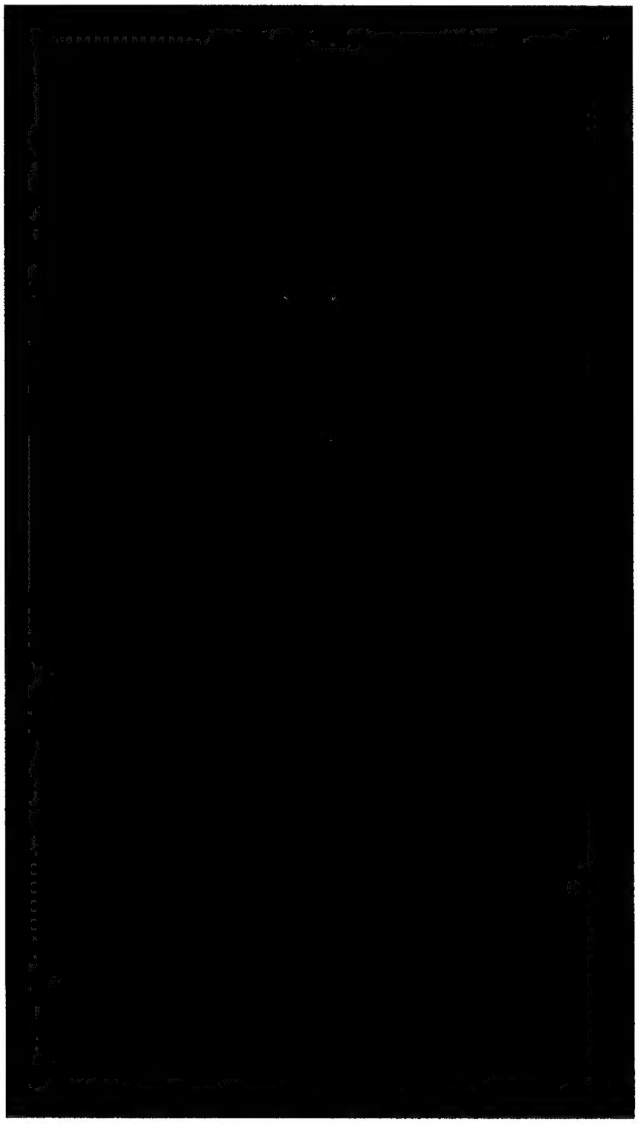

Surrey Satellite Technology Limited,
Centre for Satellite Engineering Research,
University of Surrey,
Guildford,
Surrey,
GU2 5XH, UK
Tel: +44 1483 879817
Fax: +44 1483 879503
email: d.gibbon@eim..surrey.ac.uk

VFP Hybrid Rocket

1. INTRODUCTION

The following testing was carried out in support of the Surrey Space Centre (SSC) Alternative Geometry Hybrid Rocket research and development program. The work was performed with partial funding from the European Office of Aerospace Research and Development under contract reference number F61775-00-WE036.

The testing was performed between 01/08/00 and 01/04/01 at the SSC Westcott facility, Westcott, Bucks, using the SSC rocket test facility. This report covers all aspects of the research proposal.

1.1 Application

As the size and power requirements of electronic payloads shrink and the cost of space flight remains prohibitively high, the small, secondary spacecraft industry continues to flourish. Small, secondary space missions are so rewarding that commercial, educational and government organizations are investigating (and investing) in the technology for science, communication and defense applications. One of the last remaining negative vestiges of the small, secondary space mission is the cost associated with putting the spacecraft in an optimal data-gathering orbit; This is due to secondary spacecraft mission managers routinely trading optimal orbit selection for a low cost secondary launch and because high performance on-board propulsion options typically bring high expense and unacceptable mission risk.

Hybrid rocket technology has frequently been identified as a cost effective method to take small spacecraft from an injection orbit to an optimal operational orbit or to distribute multiple spacecraft from one launch platform to various operational orbits. However, hybrid rocket technology has emerged from a launch vehicle and missile heritage; Consequently, the design, related literature and methodology have evolved to support these purposes. Hybrid rocket technology has characteristics that would be beneficial to the small, inexpensive spacecraft market: fewer components, relatively high performance, operational flexibility, reliability, safety, and a range of green propellant options - all supporting low cost propulsion applications. Unfortunately, small spacecraft designers often find themselves at odds with packaging the characteristically long and slender rocket engine within a small, volume-constrained spacecraft.

This research is concerned with providing a hybrid rocket design that is amicable to small, inexpensive space missions while providing a capability to significantly change the spacecraft's orbit. A rocket engine with these attributes would serve to increase the number of acceptable secondary launch opportunities for a given low cost mission, improve the data gathering capability of these assets by placing spacecraft in optimal orbits and thereby increase the overall utility of the small, inexpensive spacecraft for science, defense and commercial applications. In addition, the technology provides a means to de-orbit the spacecraft after a useful mission life.

Surrey Space Centre propulsion research has identified a hybrid rocket configuration that shows great promise for inexpensive spacecraft applications. The engine employs a novel, vortex flow field that serves to artificially increase the engine's L* , reduce combustion chamber size, improve mixing of the fuel and oxidiser, provide an inherent chamber wall cooling mechanism and keep the overall geometry short and flat - a geometry conducive to small spacecraft design and integration. The alternative geometry hybrid rocket (often referred to as the Vortex Flow "Pancake" Hybrid or VFP) has been designed and tested. This report presents the test results of this innovative hybrid rocket engine, an engine designed specifically for the orbit transfer of small, secondary spacecraft.

1.2 Abbreviations

VFP - Vortex Flow "Pancake" Hybrid Rocket
HTP - High Test Peroxide (89% Degussa)
N2O - Nitrous Oxide
PMMA - Polymethyl Methacrylate / Plexiglas
PE - Ultra High Density Polyethylene
EM1 - Engineering Model 1
EM2 - Engineering Model 2
Gox - Gaseous Oxygen
L/D - Length to Diameter Ratio
O/F - Oxygen to Fuel Ratio
Isp - Specific Impulse (s)
C* - Characteristic Exhaust Velocity (m/s)
L* - Combustion Chamber Characteristic Length (m)

2. ROCKET ENGINE DESCRIPTION

The testing was undertaken on two variants of the SSC Alternative Geometry Hybrid Rocket engineering model. Figure number 1 illustrates the first generation engineering model (EM1) and figure number 2 (EM2) illustrates a flight propellant testbed that was purposely elongated for test purposes. All external engineering model hardware is fabricated of heavy gauge stainless steel to facilitate safe, trouble free testing of new hybrid rocket concept. The unique feature of this hybrid rocket configuration in comparison to conventional hybrids is its length to diameter ratio (L/D). Whereas conventional hybrids typically employ L/D's far in excess of 15, the VFP L/D is nominally less than 1. This characteristic enables the VFP to take on a flat "pancake" shape, which will be easier to accommodate on small spacecraft. The VFP employs tangential oxidiser injectors that induce a vortex "drain type" flow field within the combustion chamber.

Assembly number	ASYPROP 02-001-1	Oxidisers Tested	Gox/N_2O/HTP
Chamber pressure	Variable	Chamber Dimensions	121mm Dia, 11-50mm high
Oxidiser injectors	(1,2,4 and 18 tested)	Ambient test pressure	Atmospheric
Fuel Tested	Polymethyl Methacrylate (otherwise known as PMMA, Perspex, Plexiglas, Acrylic)		

Figure 1. Engineering Model (EM1)

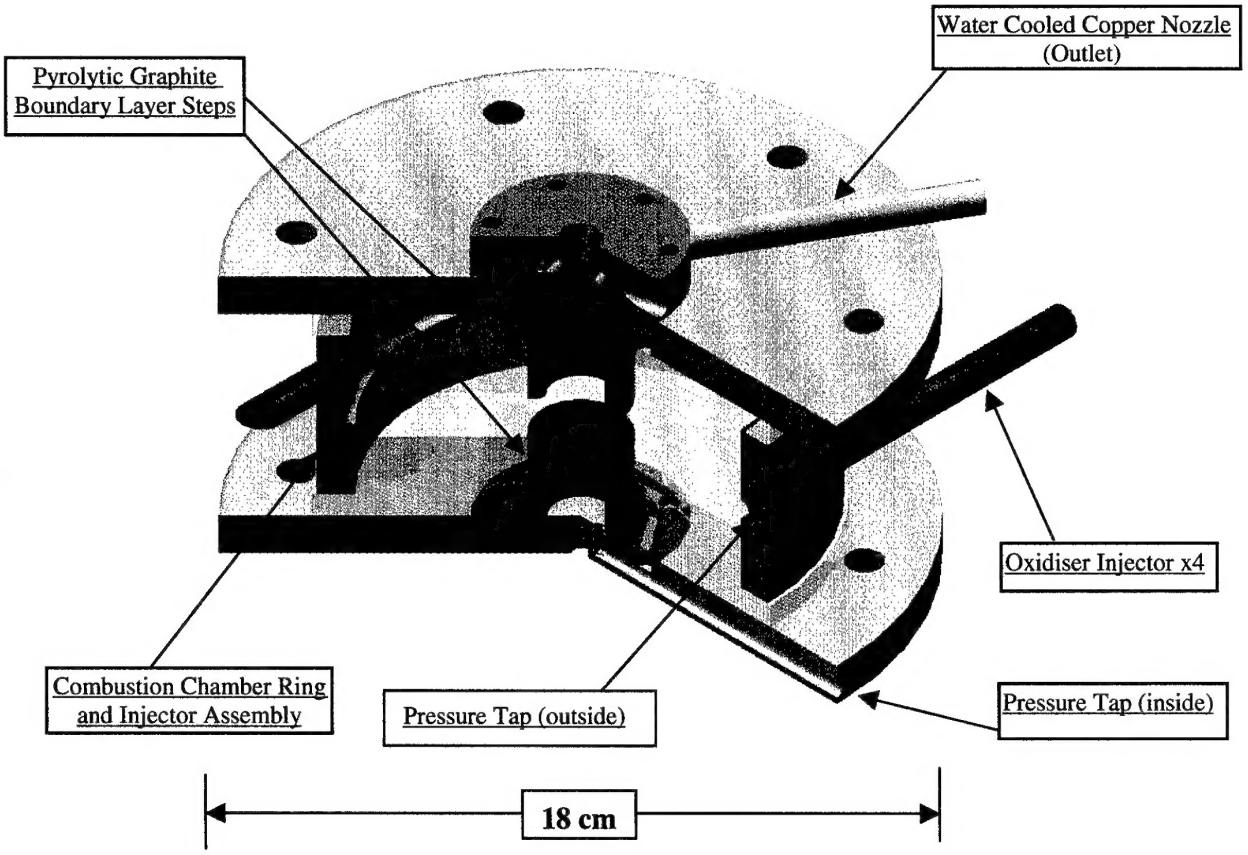

Assembly number	ASYPROP 02-001-2	Oxidiser Tested	HTP
Chamber pressure	Variable	Chamber Dimensions	100mm Dia, 20-196mm high
Oxidiser injectors	2	Ambient pressure	Atmospheric
Fuel Tested	Polyethylene		

Figure 2. Engineering Model (EM2)

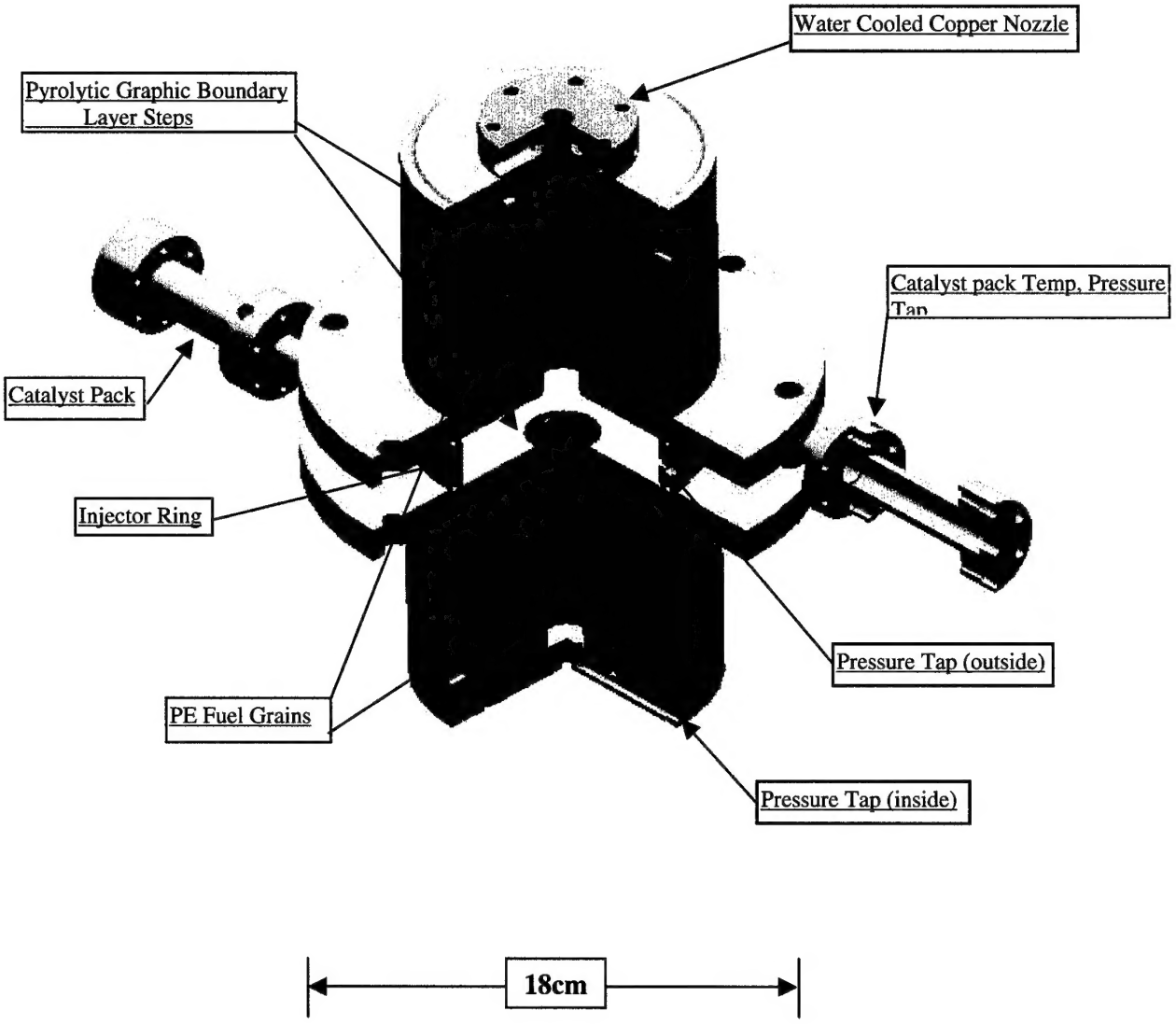

3. TEST DESCRIPTION

All VFP testing was conducted in a controlled manner to approximate (as close as possible) actual firing conditions. For instance, fuel grains - after being carefully removed and weighed were meticulously re-installed with respect to their initial position in relation to oxidiser injectors. If this were not the case, the testing would not be representative of a flight like system. Similar logic was applied throughout the alternative geometry hybrid test program.

Hybrid rockets experience a noticeable start-up and shutdown phase that can inject some uncertainty into fuel utilisation calculations. In order to minimise the uncertainty in the fuel utilisation calculations one is tempted to increase the steady-state burn duration. This test program settled on a nominal eight second burn duration in order to find a balance between minimising the influence of the start-up/shut-down phase and providing a good number of discreet "snapshots" that could be obtained from a set of fuel grains. In addition, eight seconds helped preserve the pyrolytically coated carbon boundary layer steps for multiple fuel grain sets and provided a manageable amount of data for post firing manipulation at the desired sampling speed.

3.1 Ignition and oxidiser feed

When using gaseous oxygen and PMMA, the VFP was ignited with a hot wire inserted through the nozzle. The hot wire used 3amp fuse wire with a dusting of spray adhesive and Pyrodex powder. Upon applying a 28v/10A excitation signal, the ignitor would momentarily flare. A similar ignition procedure was used for igniting the engine for N_2O operations. HTP operations entailed passing the pressurised oxidiser through a catalyst bed of silver wire mesh. The catalytic decomposition of the HTP releases superheated steam (~600C) and oxygen, spontaneously igniting the solid PE fuel.

Gaseous Oxygen and N_2O:

Test firing would begin with the subject oxidiser being regulated down to the specified test pressure. Oxygen would enter a variable area flow meter were pressure, temperature and flow rate were measured (temperature and pressure measurements were later used to correct flow meter measurements to "standard" conditions). During N2O operations, N2O flow was measured with a coriolis flow meter. The oxidiser flow was then subdivided into a primary firing valve and a (low flow) bypass valve to facilitate ignition. The low flow provided approximately 1 gram/second flow rate while the ignition circuit was energised (igniting the rocket engine), within a fraction of a second, the primary oxidiser flow valve was opened and the engine would quickly ramp up to operational parameters. The primary oxidiser line employed a variable choke (needle valve) to isolate the oxidiser feed pressure from the combustion chamber pressure and thereby reduce the probability of feed system induced pressure oscillations. After firing for the specified duration of the test, the firing valve would be closed and the all oxidiser flow would stop. A nitrogen purge was then employed to ensure the engine was extinguished and expel any un-combusted oxidiser and fuel.

High Test Peroxide:

Test firing would begin with the liquid oxidiser being pressurised to the specified test pressure using compressed nitrogen. From the main HTP tank the oxidiser would enter a coriolis flow meter prior to splitting to the two HTP catalyst packs. Prior to entering the catalyst packs, each HTP stream would pass through the needle valve and the firing valve. The needle valve was used to isolate the oxidiser feed pressure from the combustion chamber pressure (and thereby reduce the probability of feed system induced pressure oscillations). Upon entering the catalyst packs the HTP would rapidly decompose into superheated steam and oxygen and immediately enter the combustion chamber, igniting the rocket engine. After firing for the specified duration of the test, the firing valves would be closed and the all oxidiser flow would stop. A nitrogen purge was then employed to ensure the engine was extinguished and expel all HTP and non-solid fuel from the catalyst packs and the combustion chamber.

3.2 Test and data acquisition infrastructure

Figure 3 outlines the VFP gaseous oxygen test infrastructure. Oxidiser flow control was conducted via a hand operated bottle shut off valve, a hand operated pressure regulator, two pneumatic valves and a hand adjusted (needle) choke valve. Instrumentation consisted of a Bailey Fischer and Porter variable area oxygen flow meter, a 20kg Tedea Hunt Leigh load cell, 4 Gems Sensors pressure transmitters and 2 k-type thermocouples. With the exception of the load cell, all instrumentation provided a 4 to 20 mA signal to a National Instruments data acquisition board (the load cell provided a 0 to 5 volt signal). All instrumentation used screened leads and were powered by lead acid batteries to reduce electronic noise.

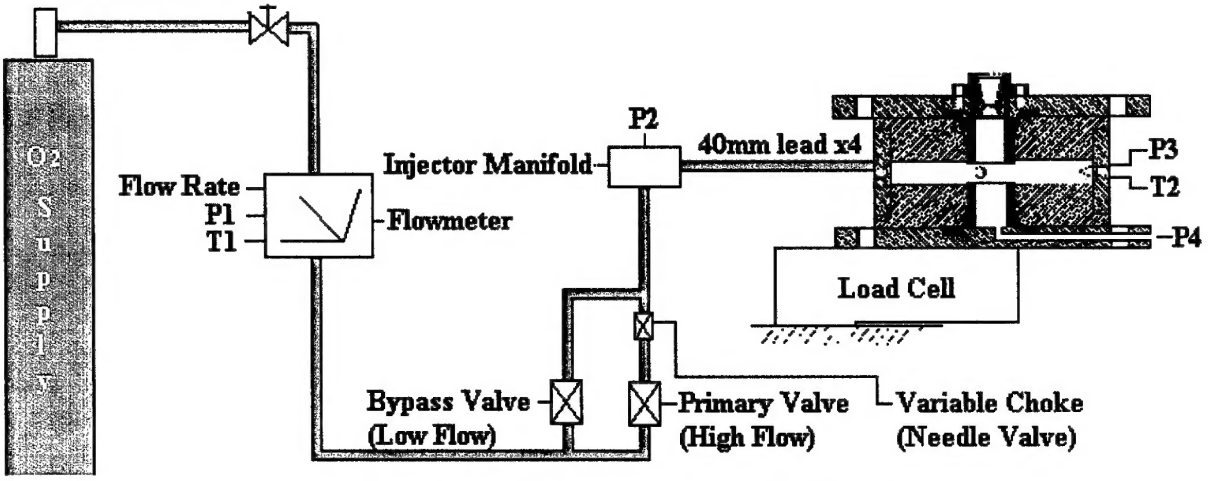

Figure 3. VFP Gox/PMMA Test infrastructure

Figure 4 illustrates the VFP HTP test infrastructure. Oxidiser flow control was conducted via a hand operated bottle shut off valve, a hand operated pressure regulator, two pneumatic valves and two hand adjusted (needle) choke valves. Instrumentation consisted of a Coriolis mass flow meter, a 30kg Tedea Hunt Leigh load cell, 5 Gems Sensors pressure transmitters, 1 Kulite high frequency pressure transducer, and 3 k-type thermocouples. With the exception of the load cell and high frequency transducer, all instrumentation provided a 4 to 20 mA signal to a National Instruments data acquisition board (the load cell and transducer provided a 0 to 5 volt signal). All instrumentation used screened leads and were powered by lead acid batteries to reduce electronic noise.

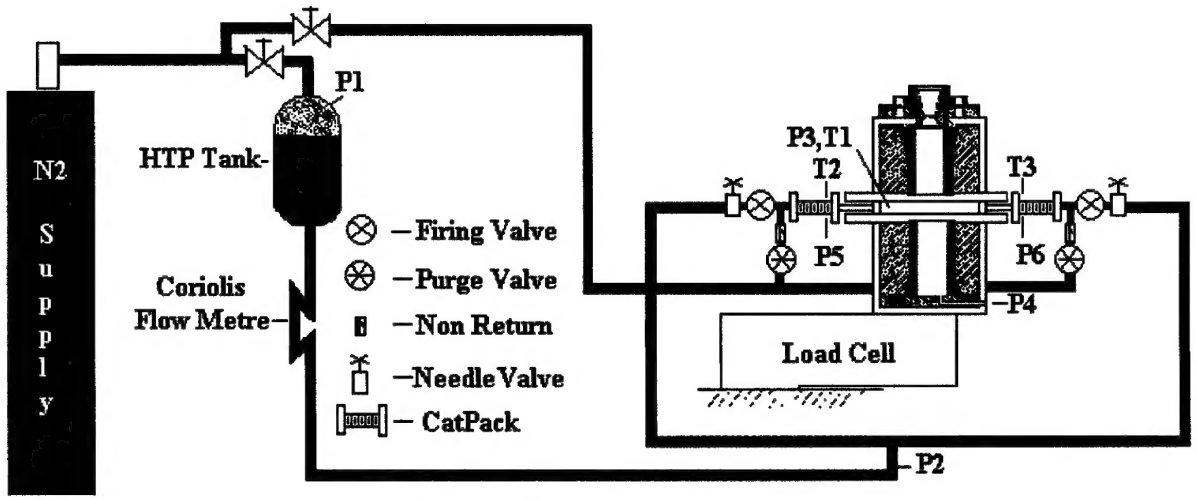

Figure 4 HTP Test Infrastructure

The National Instruments data acquisition card (DAQ) was housed within a Pentium PC operating at 233 Mhz. The DAQ card is capable of recording at 200k samples per second across a maximum of 16 data channels. Nominally, the DAQ was operated at 300 samples per second. The only instrumentation requiring such a fast sampling speed was the pressure transmitters. While a sampling speed as high as 2k samples per second would be useful for recording potential combustion instabilities within a hybrid rocket, the low cost (~£100.00) pressure transmitters were not capable of responding at speeds faster than 300hz. Later in the research program, a high frequency pressure transducer was used to assess high frequency pressure oscillations during HTP operations; this transducer was rated by the manufacturer as having a 5kHz response time. Table 1 lists instrumentation calibration parameters. Chart 1 illustrates a typical, raw, hot firing trace using gaseous oxygen and PMMA.

Instrumentation	Calibration Source	Accuracy (demonstrated)
Pressure Transmitters	Calibrated Test Gauge	0.25%
Thermocouples	Calibrated Thermocouple Simulator	0.1%
Load Cell	Calibration Weights	0.3%
Fuel Scale	Calibration Weights	0.03%
Gox Flow Meter	Factory Calibrated	2.5 %
HF Pressure Transducer	Calibrated Test Gauge	0.2%
HTP Mass Flow Meter	Factory Calibrated	0.4%

Table 1. Instrumentation Calibration Details

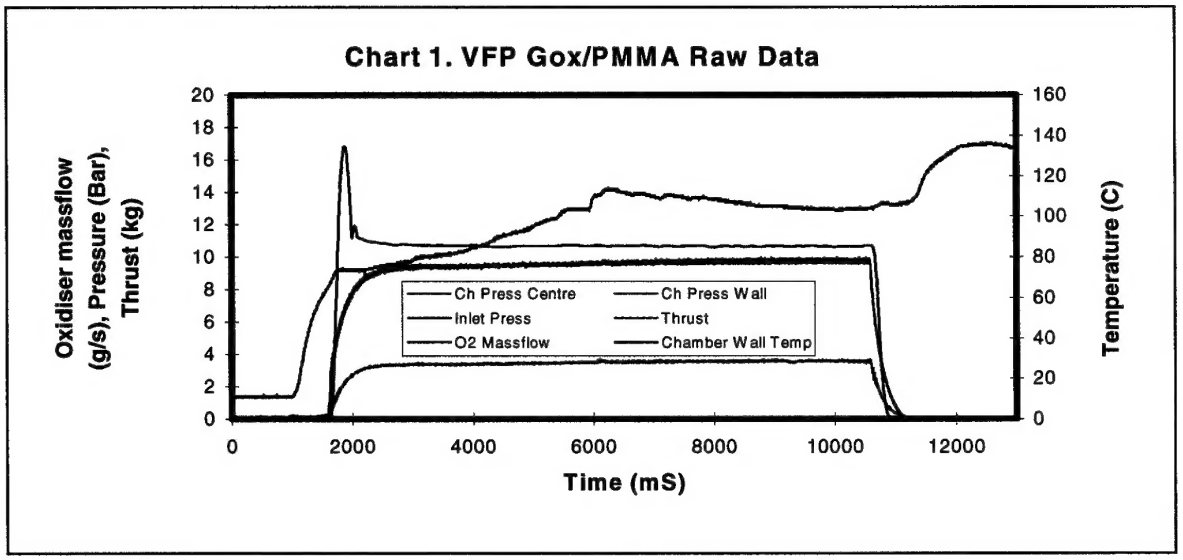

3.3 Performance Characterisation

Characteristic exhaust velocity (C*) measurements were the primary source of performance data in the VFP research program. C* measurements provide a measure of combustion chamber performance based on chamber pressure, propellant mass flow rate and nozzle throat area (equation #1). Measured C* can then be compared with theoretical values in order to determine combustion chamber efficiency (theoretical performance was calculated using the USAF "Isp" thermochemical computer code). Combustion chamber efficiency provides an indication of how well everything performs upstream of the rocket nozzle, and this is where the concern lies for an all-new rocket geometry.

Specific impulse (Isp) is the industry standard term for quoting rocket performance. Isp (equation 2) is a measure of overall (combustion chamber and nozzle) rocket performance. Since this rocket research and development program was decidedly low cost, vacuum firings and high cost rocket nozzles were not acceptable expenses. Therefore, a low cost approach was employed. Thrust (at ambient test conditions) was measured using a simple load cell mounted under the engine and firing the engine downward against it. After experimenting with steel, pyrolytically coated graphite, and copper nozzle designs, it was decided to use water-cooled copper nozzles to stand up to the extreme heat of combustion. The water-cooled nozzles employed conical (15 degree - half angle) diverging sections to keep machining costs low. The water-cooling effectively preserved the nozzle for multiple firings. However, the active cooling extracted up to 18% of the exhaust stream's energy (~7.3Kw), necessitating correction of the measured Isp data. Equation 3 illustrates the calculation of the correction factor for nozzle energy loss.

In order to minimise the influence of start-up and shutdown transients on performance measurement, all performance measurements were averaged over one second (half way through each run). The halfway mark also corresponds most accurately with the average fuel mass flow rate (calculated post firing).

$$C^* = \frac{PcAt}{\dot{M}t} \qquad \text{Equation \#1}$$

Where: Pc is chamber pressure - absolute (Pa)
At is the nozzle throat area (M^2)
$\dot{M}t$ is the total propellant mass flow (kg/s)

$$Isp = \frac{F}{\dot{M}tgo} \qquad \text{Equation \#2}$$

Where: F is rocket thrust (N)
$\dot{M}t$ is the total propellant mass flow (kg/s)
go is the acceleration of gravity ($9.81 m/s^2$)

$$Cf = \frac{Pabs}{Pgen} = \frac{\dot{m}w * cv * \Delta T}{\frac{F * C}{2}} \qquad \text{Equation \#3}$$

Where: Cf - Correction Factor
Pabs - Power absorbed by the water (w)
Pgen - Power generated by the engine (w)
$\dot{m}w$ - water mass flow rate (kg/s)
cv - specific heat of water (J/kg°K)
ΔT - temperature change of water (°K)
F - rocket thrust (N)
C - rocket exhaust velocity (m/s)

3.4 Fuel utilisation sensitivity analysis

This phase of the VFP research concentrates on fuel utilisation (using oxygen and PMMA) and as such relies on sound measurement principles. Fuel flow measurement was conducted by weighing the fuel grains (to within a tenth of a gram) before and after each firing, the amount of fuel used would then be divided by the duration of the firing in order to establish the average fuel mass flow rate in grams per second. Several factors were tested in order to gauge their effect on solid fuel mass flow rate, among them are oxidiser mass flow rate, internal engine geometry, oxidiser injection velocity, number of oxidiser injectors, and chamber pressure effects. Table 2 provides an overview of parameters measured, parameters varied and number of firings.

PARAMETER OF OBSERVATION	CONFIGURATION NUMBER OF INJECTORS	INJECTOR DIAMETER	NOZZLE DIAMETER	NUMBER OF FIRINGS	NOTES:
O2 MASS FLOW EFFECTS	4	6.5MM	4MM	7	CONSTANT PC
	4	6.5MM	5MM	7	SLIGHT VARIATION IN INVEL
	4	6.5MM	6MM	7	
GEOMETRY EFFECTS	4	6.5MM	6MM	13	SMOOTH GRAIN SURFACES
NUMBER OF INJECTOR EFFECTS	1	6.5MM	6MM	9	CONSTANT MO
	2	5.0MM	6MM	7	
	4	3.3MM	6MM	10	
& INJECTION VELOCITY EFFECTS	1	3.3MM	6MM	3	CONSTANT PC
	1	6.5MM	6MM	2	
	2	3.3MM	6MM	3	
	2	6.5MM	6MM	3	
	4	3.3MM	6MM	3	
	4	6.5MM	6MM	3	
	18	3MM	6MM	15	INJECTOR RING FIXTURE
CHAMBER PRESSURE EFFECTS	4	6.5MM	4MM	6	CONSTANT MO
	4	6.5MM	5MM	9	
	4	6.5MM	6MM	10	
FUEL UTILISATION FIRINGS				127	TOTAL

Table 2. Parameters tested for effect on fuel mass flow

3.4.1 PROCEDURES

As previously mentioned, there were five distinct parameters that were individually isolated in order to determine their effect on solid fuel utilisation. Oxidiser mass flow, chamber geometry, number of injectors, injector velocity and chamber pressure. This section will detail how these measurements were made.

3.4.1.1 Oxidiser mass flow effects

In order to accurately gauge the effect of oxidiser mass flow on fuel mass flow rate one needs to isolate all other effects or understand them well enough to "normalise" their effect. Changing oxidiser mass flow for a given engine configuration will change injection velocity, and chamber pressure. In addition, the chamber geometry changes during consecutive runs necessitating careful consideration of how this parameter affects the oxidiser mass flow results.

3.4.1.2 Chamber Geometry

Chamber geometry refers to the gradually increasing height of the combustion chamber as the fuel grains are consumed. As the fuels grains are consumed, the grains recede away from each other changing the height, volume and aerodynamic characteristics of the combustion chamber. While other characteristics (oxidiser mass flow rate, injection velocity, number of injectors, chamber pressure) were kept constant, firings were conducted with fuel levels representative of different levels of consumption while fuel liberation (in g/s) was measured. In order to negate the possibility of other factors (surface imperfections, vortex patterning) influencing the geometry measurements, the fuel grains were machined flat for each consecutive eight-second firing. Figure 5 represents five different levels of fuel grain utilisation that were simulated (with machined fuel grains) during this test (note: the figure illustrates 1 fuel grain, keep in mind there was an identical fuel grain (horizontally opposed) during each firing).

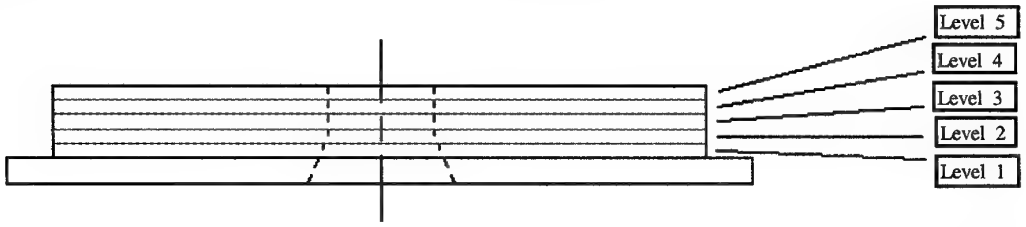

Figure 5. Side view of a fuel grain illustrating various levels representative of different levels of fuel consumption

3.4.1.3 Number of injectors

The VFP engineering model hardware provided for four separate oxidiser injectors. The injectors could be capped to provide one, two or four injector configurations. While oxidiser mass flow, chamber pressure and geometry could be easily controlled, injection velocity varied with the sum of the cross sectional areas of the total number of injectors used. Therefore, relevant injection velocities were recorded in order to normalise the effect of injection velocity with respect to the number of injectors.

In addition, a multiple (18) injector fixture was tested. The fixture (figure 6) was inserted within the combustion chamber against the chamber wall (aligned with the four fixed oxidiser injectors).

Figure 6. Multiple Injector Fixture

3.4.1.4 Injector Velocity

Injection velocity was determined by the mass flow rate of oxidiser (at a specific density) through the sum of the injector cross sectional areas. In addition to the variable cross sectional injector area afforded by multiples of injectors (1,2,4), chokes were made-up to further vary the injector area. The chokes would vary individual injector area discretely, affording the choice of 8.55mm^2, 19.63mm^2, and 33.18mm^2 injectors. See figure 7.

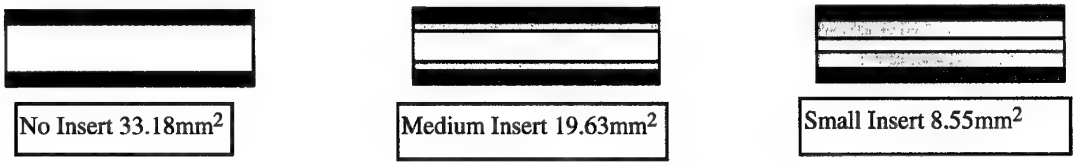

Figure 7. Variable injector (choke) fixtures.

3.4.1.5 Chamber pressure

Keeping other parameters constant while changing nozzle throat diameter provided a means to isolate the effects of chamber pressure on fuel liberation. Water-cooled copper nozzles were manufactured in 4, 5 and 6mm dia sizes and oxidiser mass flow rate was adjusted to appropriate (constant) levels. The pressure series firings were conducted and fuel liberation was calculated.

3.5 Combustion chamber pressure mapping

Combustion chamber pressure mapping was conducted to determine the presence of a cyclostophic pressure drop across the combustion chamber. This is accomplished by recording pressures at the periphery of the rocket engine (near the injectors) and at the centre of the engine (opposite the nozzle).

3.6 Engine scalability investigation

Engine scalability is investigated by decreasing the overall size of the fuels grains and determining if fuel utilisation and performance track with the decrease in size.

4. EXPERIMENTAL RESULTS

4.1 Performance

Although procedures and apparatus were designed to provide the highest degree of accuracy possible, all performance testing was conducted in a low cost environment. Subsequently, the performance figures quoted in this report are intended to demonstrate the potential of this new rocket technology rather than demonstrate ultimate performance achievable.

4.1.1 CHARACTERISTIC EXHAUST VELOCITY

Characteristic exhaust velocity or "C*" (see equation. 1) was used to determine combustion efficiency on select VFP firings. C* was the preferred performance metric in the research program for two reasons; first, C* is based on (relatively) easily obtained quantities (absolute chamber pressure, throat area and total mass flow rate), these parameters are difficult to refute. Secondly, C* focuses on the novel aspect of the research, the alternative geometry combustion chamber rather than the performance downstream of the low-cost, conventional nozzle where inefficiencies, and losses need to be measured and/or estimated.

Combustion efficiency was determined by dividing measured C* values by theoretical values (calculated on the USAF "Isp" thermochemical computer program) to determine the percentage of theoretical achieved. The individual C* measurements were compared with Isp code results using the same chamber pressures and O/F ratio as the actual run. Chart 2 illustrates measured and theoretical values as well as efficiency for 166 Gox/PMMA firings; error bars indicate all firings were within a 5% of theoretical values (i.e. all measurements exceeded 95% of theoretical combustion efficiency). The high combustion efficiency is attributed to the centripetal acceleration within the combustion chamber and the enhanced mixing of fuel and oxidiser within the vortex flow field.

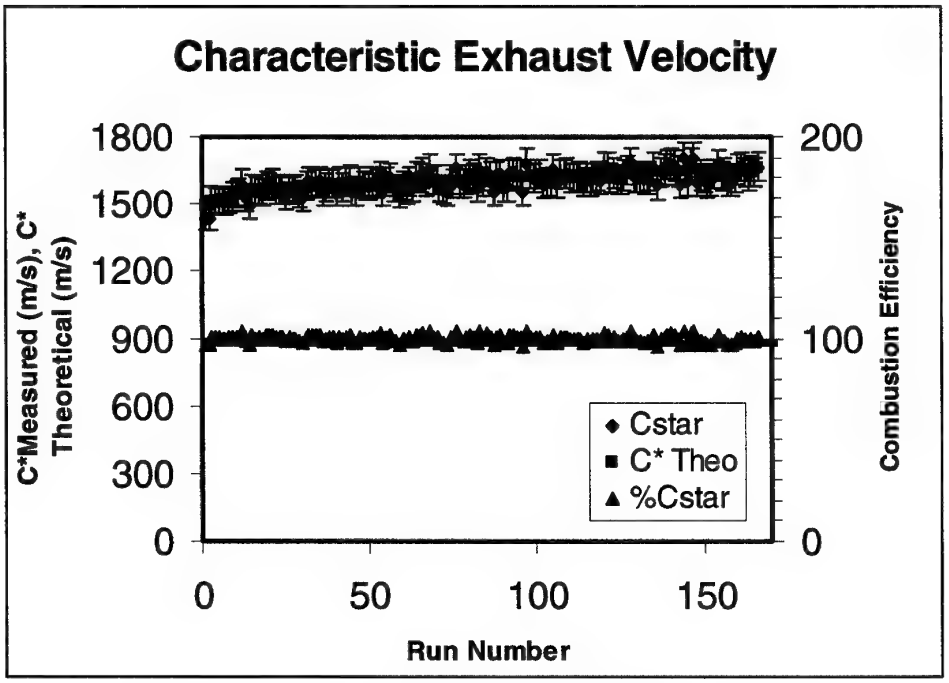

Chart 2. Theoretical and Actual Combustion Efficiency Comparison

In order to perform a "sanity check" of the experimental accuracy, a histogram of the experimental data was plotted (chart 3) the data demonstrates a normal distribution around the average value of 99.7%.

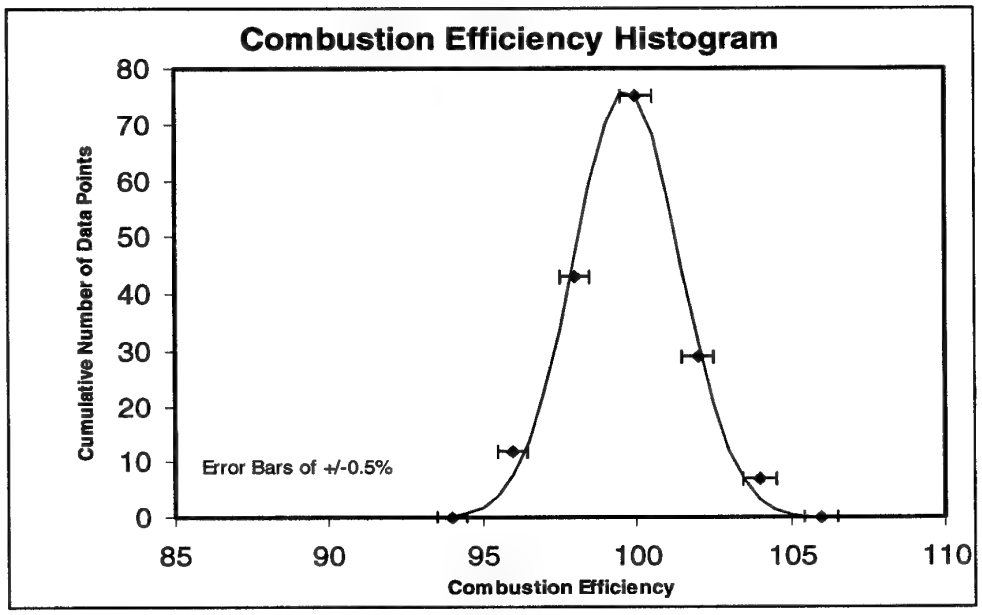

Chart 3 Combustion Efficiency Histogram

4.1.2. SPECIFIC IMPULSE MEASUREMENTS

Although specific impulse is relatively straightforward to measure (equation 2.6), it is not the metric of choice for a low cost rocket research and development program. Engine thrust measurement is highly dependant on combustion performance, thrust alignment, nozzle design/efficiency and expansion conditions. Since all testing was conducted in atmospheric conditions with a conical nozzle, one would expect performance much lower than theoretical values. Actively cooling the rocket nozzle was the only method found to cost-effectively maintain the integrity of copper nozzle throat (and thus the accuracy of C* measurements), figure 8. The cooled nozzles performed exceptionally well, preserving the nozzle throats throughout the research program. However, the coolant water extracted up to 7Kw from the exhaust stream during operation, robbing approximately 18% of the generated power.

Isp was measured for 84 separate firings (Chart 4) and compared with theoretical values (provided by the USAF "Isp" thermo-chemical code). The theoretical values are calculated based on the same O/F ratio, chamber pressure and ideal expansion through a nozzle to ambient conditions. After correction for the effects of the water-cooled nozzle, the VFP achieved an average of 93% of theoretical Isp (note: correction from a 15° half-angle conical nozzle to a bell nozzle should yield an additional 1.7%); individual Isp results are tabulated in table 6.2.

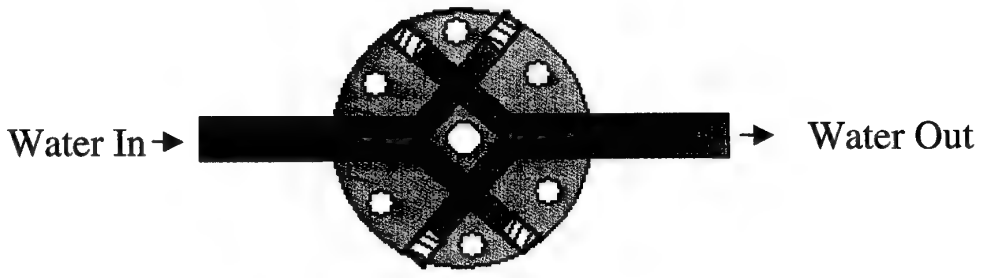

Fig.8 Cutaway view (at throat) of water-cooled copper nozzles

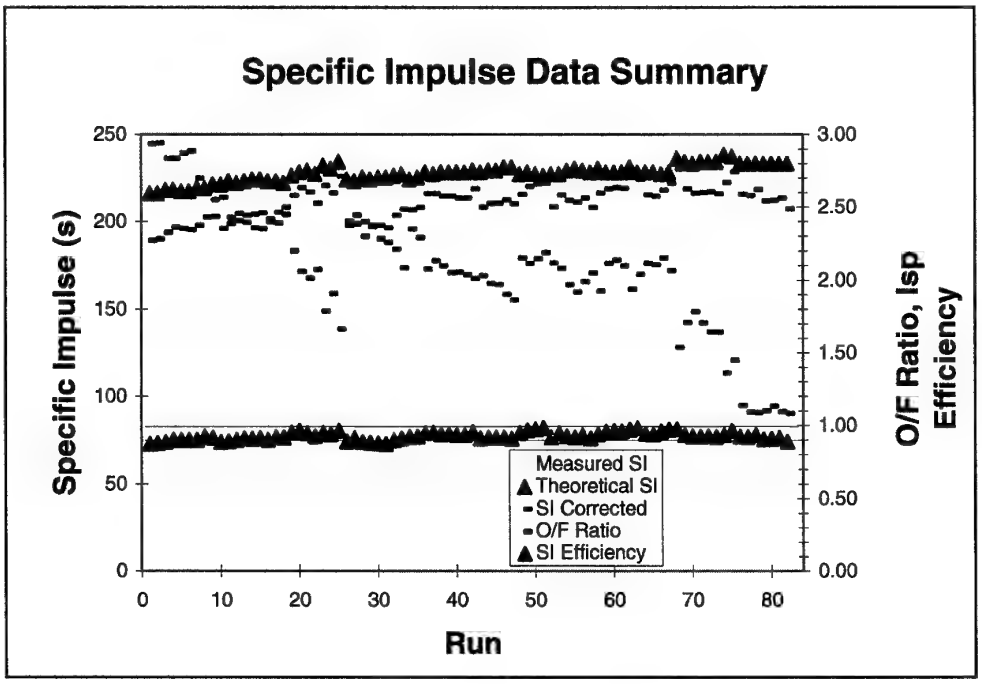

Chart 4. Isp vs. Theoretical Values

Once again, a histogram of the experimental data was used to establish confidence that the data was methodically collected and that glaring procedural errors were not introduced; the histogram illustrates a normal distribution about the average value of 93%. Although tighter result grouping would have been preferred, the results are judged to be consistent with a low cost approach to thrust measurement (Chart 5).

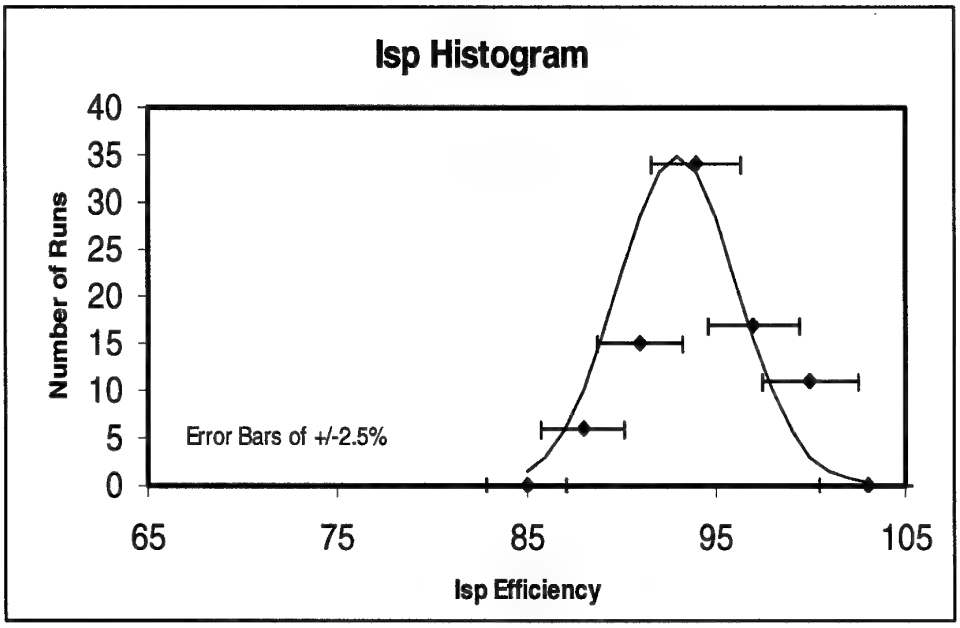

Chart 5. Illustrates a normal distribution of the Isp measurements around the average of 93% (of theoretical values).

4.2 Fuel utilisation sensitivity analysis

4.2.1 OXIDISER MASS FLOW EFFECTS

The oxidiser mass flow ($\dot{M}$ o) effects on fuel consumption were measured by increasing $\dot{M}$ o as other parameters were kept constant. In order to keep chamber pressure constant over the three-oxidiser mass flow regimes, the rocket nozzle throat area was changed by substituting various nozzles into the test apparatus. This arrangement provided a capability to vary oxidiser mass flow by 66% while maintaining chamber pressure variation within 10%, small chamber pressure variations were deemed insignificant. Every effort was made to keep injector velocity variation low over the regimes tested; however, the discrete nature of the test apparatus prevented precise control of the injector velocity parameter. As expected, $\dot{M}$ o did proportionally effect fuel consumption within VFP. However, it appears that the injection velocity did effect the measurement (injection velocity did vary from 2.3m/s to 6.7 m/s over the regimes tested). Chart 6.6 illustrates a nearly linear increase in fuel mass flow rate with increasing oxidiser mass flow rate (each data point represents the average of 7 firings). However, the influence of injection velocity can still be seen, this would explain the reluctance of the linear relationship between the oxidiser and fuel mass flow rates to intersect with the chart's origin; section 4.2.4 covers injection velocity in more detail, demonstrating that fuel liberation rate is highly sensitive at low oxidiser injection velocities.

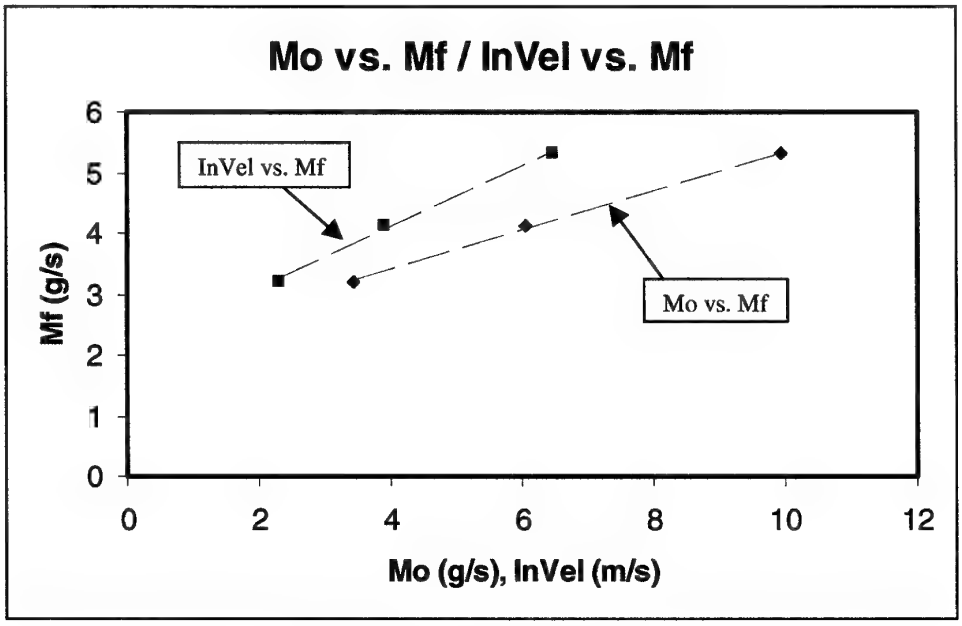

Chart 6. Oxidiser Mass Flow Effects

4.2.2 CHAMBER HEIGHT EFFECTS

Chamber height effects looked specifically at the change in fuel mass flow rate as the fuel grains were consumed; as the fuel grains are consumed the combustion chamber height increases from 1.2cm (initial conditions) to 5cm (final condition), equating to a chamber volume change of greater than a factor of 4. In order to negate the effects of fuel grain patterning and get pure geometry-effect measurements, fuel grains were machined smooth to represent gradually increasing chamber height (figure 5 illustrates the different levels tested).

Unexpectedly, the geometry measurements did not exhibit any definitive trends in regard to fuel liberation over the chamber height range tested (1.2 to 5cm). Table 3 provides insight into how well the parameters could be controlled with the test infrastructure while chart 7 illustrates the insensitivity between chamber height and fuel mass flow rate. Chart 8 presents fuel mass flow measurements for 13 geometry-based firings (at varying chamber heights); Average deviation was 2.1% from the mean.

Run	Inj Vel	Mo	Mf	Pc	Initial
	m/s	g/s	g/s	Bar	Thickness
					mm
1	6.59	11.23	5.3	8.37	21.40
2	6.62	10.90	5.2	8.25	17.80
3	6.83	11.22	5.2	8.36	14.20
4	6.69	11.17	5.1	8.43	10.60
1	6.68	10.94	5.2	8.24	17.80
2	6.90	11.18	5.2	8.17	14.20
3	6.78	11.21	5.4	8.36	10.60
4	6.48	10.92	5.5	8.53	10.60
1	6.91	11.33	5.5	8.48	21.40
2	6.98	11.28	5.4	8.34	17.80
3	7.14	11.38	5.4	8.22	14.20
4	7.16	11.38	5.3	8.19	10.60
5	6.88	11.08	5.4	8.31	7.00

Table 3. Tabulated Geometry Measurements

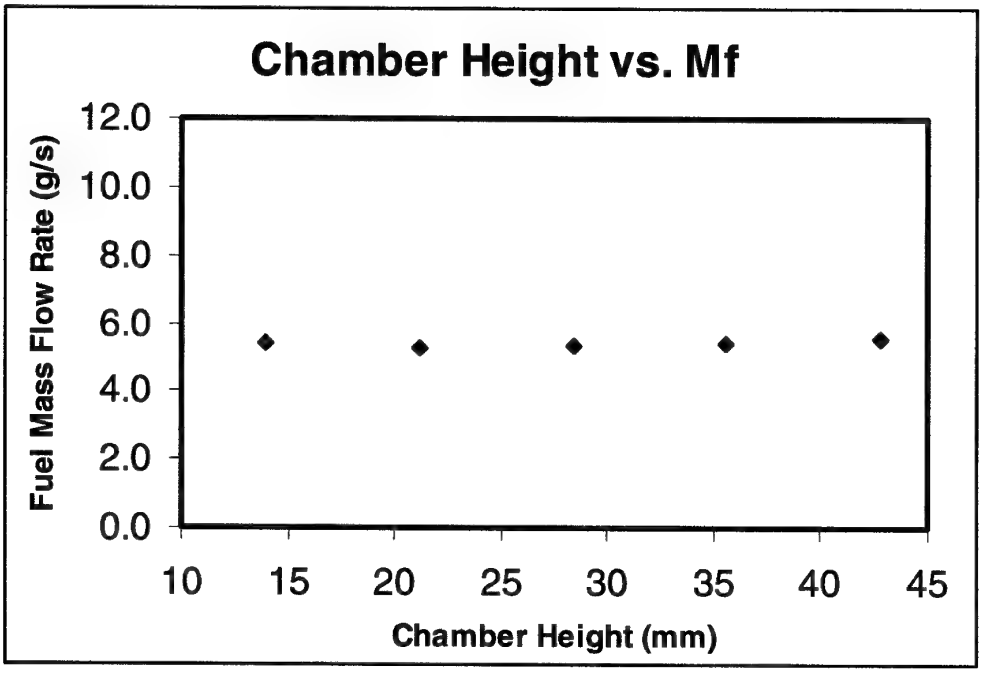

Chart 7. Combustion Chamber Height vs. Fuel Mass Flow Rate

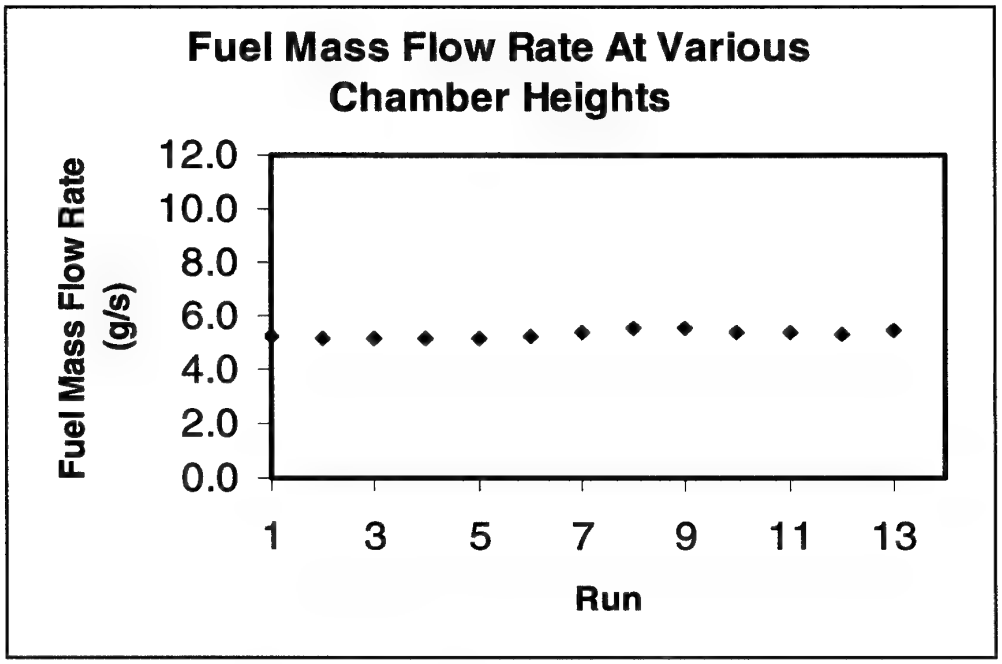

Chart 8. Fuel Mass Flow Rate for 13 Flat Grain Firings

In addition to the previously identified parameters, the fuel grain surface (on the top and bottom fuel grains) was noted to take on a "vortex pattern" that became progressively pronounced on subsequent firings of the same fuel grain (figure 9). As the vortex pattern became more pronounced the fuel mass flow rate increased; the increase in fuel mass flow rate is attributed to the increase in fuel surface area and enhanced convective heat transfer to the fuel grain surface.

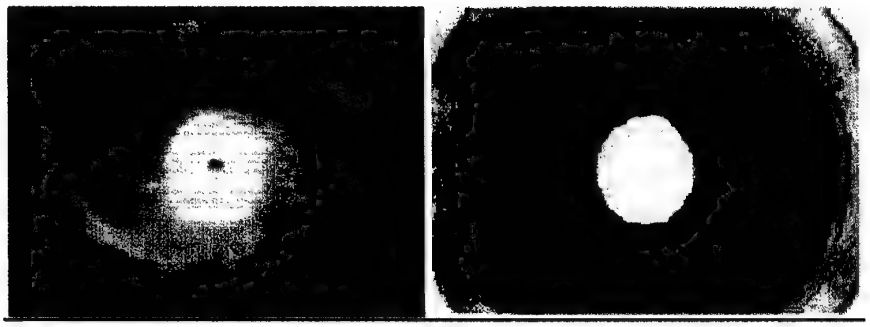

Figure 9. Fuel Grain Patterning (a) during firing (b) post firing

Certain parameters were determined to affect the rate at which the patterning appeared (injection velocity and number of injectors). In order to illustrate the patterning effect, results from two experimental configurations are compared; the first configuration allowed the vortex patterning to develop over 13 firings. The second sequence of thirteen firings had the patterning artificially removed (machined flat), the results of these firings are shown in chart 9. In the following sections, certain trends and data sets include the effects of the vortex enhanced fuel mass flow rate while others avoid the effect by using data from the first firing of a fuel grain set or by using machined grains (machined flat) prior to subsequent firing; the following sections will identify weather the effect is present in the data or not. The combined effect of the increasing turbulence and fuel area results in an increasing fuel mass flow rate and decreasing O/F ratio over the duration of the fuel grain life. While conventional hybrids have shown to vary O/F by as much as 32% over the duration of a 50second burn [Humble 95], Chart 9 illustrates a VFP O/F variation of less than 13% over a 50 second run (and the VFP can be configured to provide less of a O/F shift than illustrated).

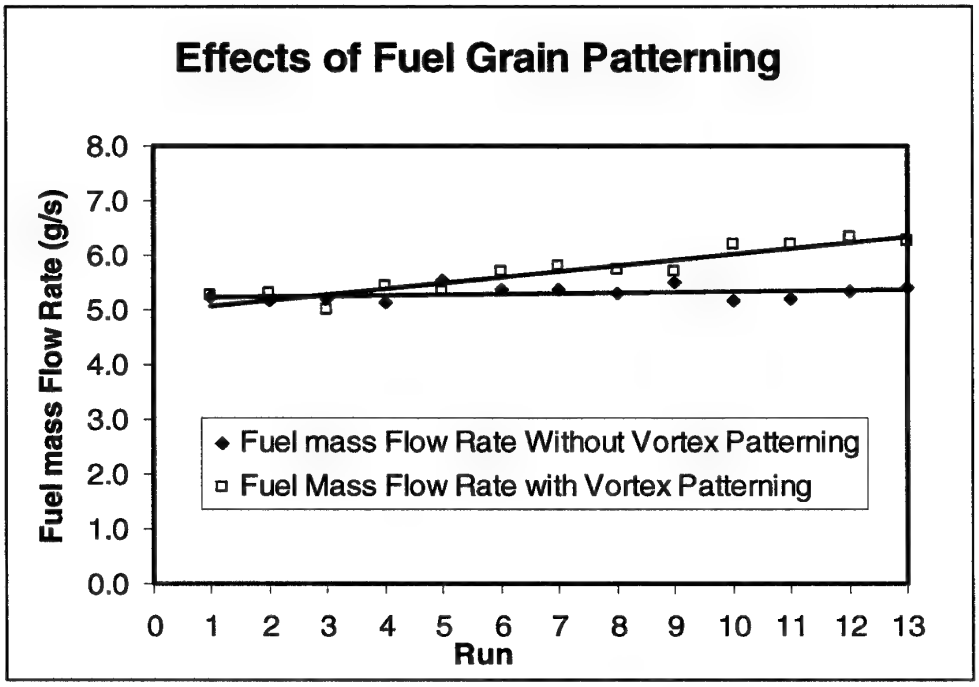

Chart 9. Fuel Grain Patterning Effects on Fuel Mass Flow Rate

4.2.3 NUMBER OF INJECTOR EFFECTS

The number of injector's metric was difficult to isolate from injector velocity metric for a constant oxidiser mass flow rate. Unfortunately, the test apparatus had a limited number (3) of discreetly sized injector chokes (see section 3.4.1.4) making it difficult to match the same cross-sectional area for different numbers of injector configurations (1,2,4). Three configurations did provide similar cross sectional areas (Table 4) providing a means to produce some comparative data.

CONFIGURATION	INJECTOR AREA
1 Injector 6.5 mm choke	$33mm^2$
2 Injector 5mm choke	$39mm^2$
4 Injector 3.3mm choke	$34mm^2$

Table 4 Similar area injector configurations

One of the first observations to be recorded during the "number of injector" firings was that fewer injectors produced more pronounced "vortex patterning" and the rate at which the pattern formed on the fuel grains accelerated. Previous firings provided evidence for a higher fuel mass flow rate with increased fuel grain patterning. Table 5 illustrates the enhanced fuel mass flow associated with fewer injectors.

CONFIGURATION	$\dot{M}_O$	$\dot{M}_F$
1 injector	10.15	7.2
2 injector	10.6	7.1
4 injector	10.9	6.3

Table 5. Increasing Fuel mass Flow with Fewer Injectors (averaged)

Note: Oxidiser mass flow was intended to remain constant. Increased oxidiser mass flow has been shown to enhance fuel mass flow; this effect was "overpowered" by the increased turbulence and vortex patterning effect associated with fewer injectors (as demonstrated in table 5). An 18 injector "multiple injection fixture" was used to drastically increase the number of injectors on EM1. Visually, one could see that additional injectors reduced the effect of the vortex patterning on the fuel grain; as expected, the large number of injectors lowered local injection velocity. Chart 10 illustrates the fuel mass

flow rate growth using the multiple injection fixture in comparison with the four-injector configuration (at the same oxidiser mass flow rate).

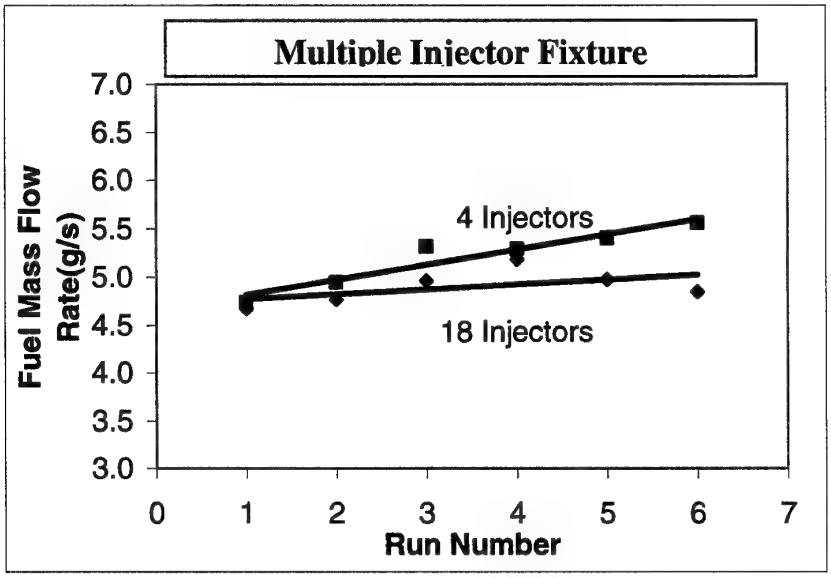

Chart 10. Multiple (18) injector vs. 4 Injector effect on fuel mass flow rate

4.2.4 OXIDISER INJECTION VELOCITY EFFECTS

Injection velocity effects were measured for each number of injector schemes (1,2,4). This was accomplished while attempting to keep other parameters constant (oxidiser mass flow rate, chamber pressure) and minimising the vortex patterning / number of injector effects (by using only the first two burns for velocity effect measurements). Oxidiser injection velocity was varied by inserting injector choke fixtures into the standard "No Insert" injector (illustrated in figure 7). Table 6 tabulates the data to demonstrate the relative amount of control on other influencing factors while chart 11 illustrates the effect of increasing oxidiser injection velocity (over a fairly large range) on fuel mass flow rate; the data implies a relatively strong relationship between injection velocity and fuel mass flow rate (especially when the injection velocity is low). In addition, the data with different oxidiser mass flow rate measurements is included (coloured in blue).

Set	Inj Vel	Mo	Mf	Pc	Notes
	M/s	g/s	g/s	Bar	
1	78.8	10.28	9.8	10.23	1 Injector, 3.3mm dia inlet choke
2	42.7	10.83	8.1	9.92	2 Injector, 3.3mm dia inlet choke
3	22.5	10.97	6.8	9.37	4 Injectors, 3.3mm dia inlet choke
4	13.6	11.27	5.8	8.23	2 Injectors, No inlet choke (6.5mm dia)
5	6.8	11.27	4.9	8.07	4 Injectors, No inlet choke (6.5mm dia)
6	6.7	9.9	5.1	7.9	4 Injectors, No inlet choke (6.5mm dia)
7	4.0	6.0	4.2	8.0	4 Injectors, No inlet choke (6.5mm dia)
8	2.3	3.4	3.2	7.7	4 Injectors, No inlet choke (6.5mm dia)

Table 6. Averaged Injection Velocity Results

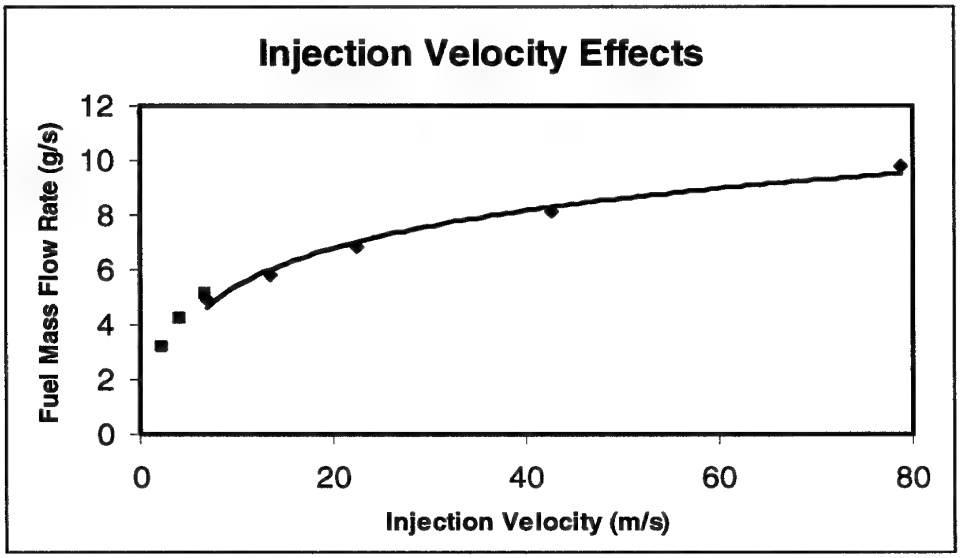

Chart 11. Oxidiser Injection Velocity vs. Fuel Mass Flow Rate

Injection velocity turned out to be a powerful tool for predicting fuel liberation within the VFP. While other parameters varied according to table 7 fuel liberation could be predicted by injection velocity alone to within 10% according to:

$$Mf = 2.9027\ (InVel)^{.2832} \qquad \text{Equation 4}$$

Where:
Mf – Fuel Mass Flow Rate (g/s)
InVel – Oxidiser Injection Velocity (m/s)

Parameter	Oxidiser Mass Flow	Injection Velocity	Chamber Pressure[1]	Injector Number
Variation	3.4 to 11.3 g/s	84.3 to 2.3 m/s	7.2 to 10.7 Bar	1, 2, or 4

Table 7. Parameter range tested to validate injection velocity relationship

4.2.5 COMBUSTION CHAMBER PRESSURE EFFECTS

Combustion chamber pressure (Pc) was varied using nozzles with 4, 5, and 6mm throat diameters. Oxidiser mass flow rate and injection velocity were controlled to within 0.8g/s and 3.61m/s respectively (table 8). Chart 12 illustrates the averaged values for 18 independent firings, demonstrating an increasing relationship between chamber pressure and fuel mass flow rate; the values were averaged to compensate for the vortex patterning effect. Note that the enhanced fuel liberation rate associated with the increasing pressure "overpowered" the injection velocity effect.

[1] Pressures noted as gauge pressure.

Set	Inj Vel	Mo	Mf	Pc	Notes
	M/s	g/s	g/s	Bar	4 Injectors, No inlet choke
1	6.50	9.93	5.3	7.86	6mm Nozzle
2	4.76	10.51	6.2	12.19	5mm Nozzle
3	2.89	10.74	6.8	21.20	4mm Nozzle

Table 8. Combustion Chamber Pressure Results

While there wasn't enough data to establish a fuel liberation equation based upon injection velocity for the higher-pressure runs, a pressure coefficient reliably adjusted the established injection velocity equation over the tested regimes according to:

$$Mf = 1.1738\ (InVel)^{.2832}(Pc)^{.4799} \qquad \text{Equation 5}$$

Where:
Mf – Fuel Mass Flow Rate (g/s)
InVel – Oxidiser Injection Velocity (m/s)
Pc – Chamber Pressure (Bar)

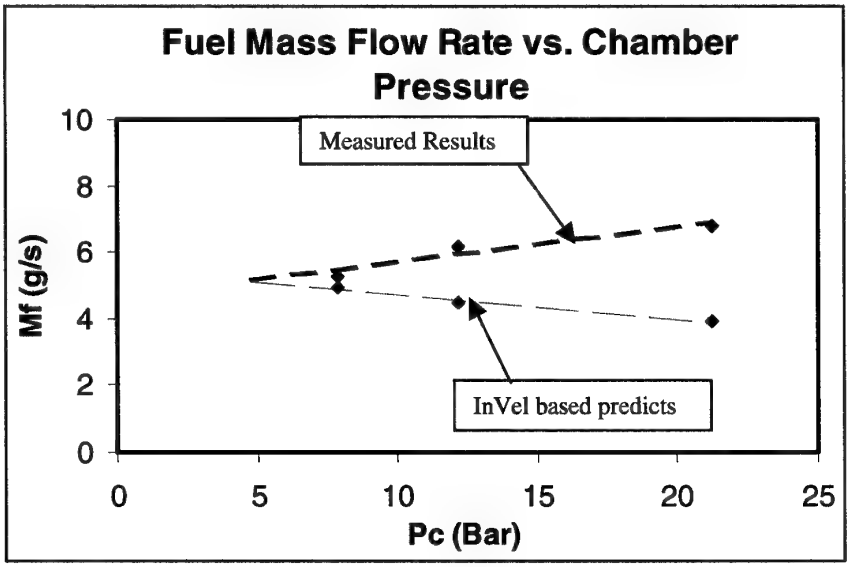

Chart 12. Combustion Chamber Pressure Effects

Fuel liberation associated with pressure is usually attributed to a radiation or combustion kinetics effects [Humble 95]. The radiation effect is largely associated with metallized fuel grains at high pressures and low oxidiser flux; whereas the kinetic effect is associated with low pressures or high mass flux. Although mass flux is not defined (in the conventional sense) within the vortex flow field, it appears that the VFP fuel liberation experiences a kinetic pressure related effect.

4.3 Chamber Pressure Mapping

Figure 10 illustrates a cutaway view of the VFP engineering model detailing the positions of two VFP pressure taps (named "inside" and "outside"). A free vortex will typically demonstrate a pressure gradient from the outside edge of the vortex to the inside of the spiral; chart 13 illustrates this effect by injecting room temperature nitrogen into the EM1 hardware and measuring the pressure gradient from the wall of the combustion chamber (outside) to the centre (inside) of the engine. Two things occur when the engine is ignited that act to diminish the pressure gradient across the combustion chamber. First, the fuel rich boundary layers (top and bottom) significantly slow the rotation of the free vortex, second, the high temperature and increased mass flow from the fuel surface act to help to diminish the combustion chamber pressure gradient across the radius of the chamber. Chart 14 illustrates this effect during a live firing; notice that during the engine start-up phase (limited combustion, limited thermal gradient, limited fuel mass flow, minimal boundary layers) the two chamber pressures are separating to establish a pressure gradient; once full combustion is established, the inside pressure trace converges with the outside trace to a indiscernible chamber pressure gradient.

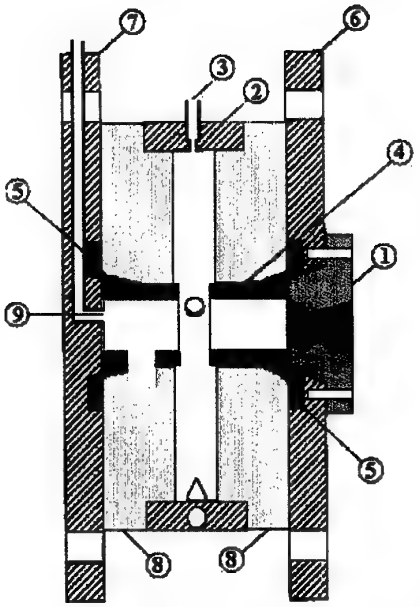

1. Water Cooled Copper Nozzle
2. Combustion Chamber Ring
3. Chamber Pressure Tap 1 (outside)
4. Pyrolytic Graphite Boundary Layer Step
5. Boundary Layer Step Fastener
6. Chamber Plate w/Nozzle Assembly
7. Chamber Plate
8. Fuel Grains (identical)
9. Chamber Pressure Tap 2 (inside)

Figure 10. EM1 Cutaway Detailing Location of Pressure Taps

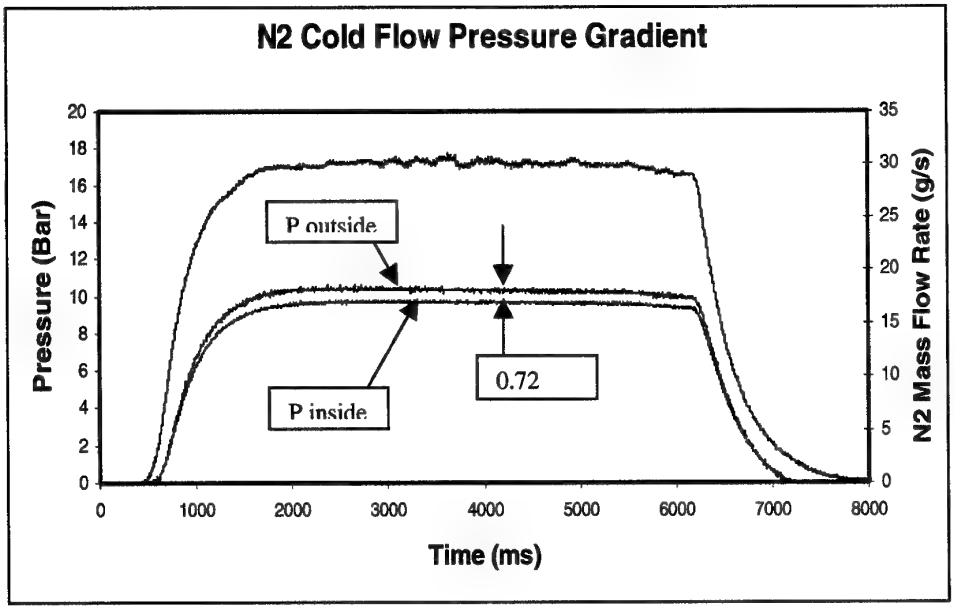

Chart 13. Cold Flow Vortex Pressure Gradient

Since the variation in combustion chamber pressure from the perimeter of the engine to the inside of the engine was very low during firings and because placing pressure taps through the fuel grain proved to be extremely tedious, spot measurements between these two extremes were deemed to be not worth expending the limited research resources.

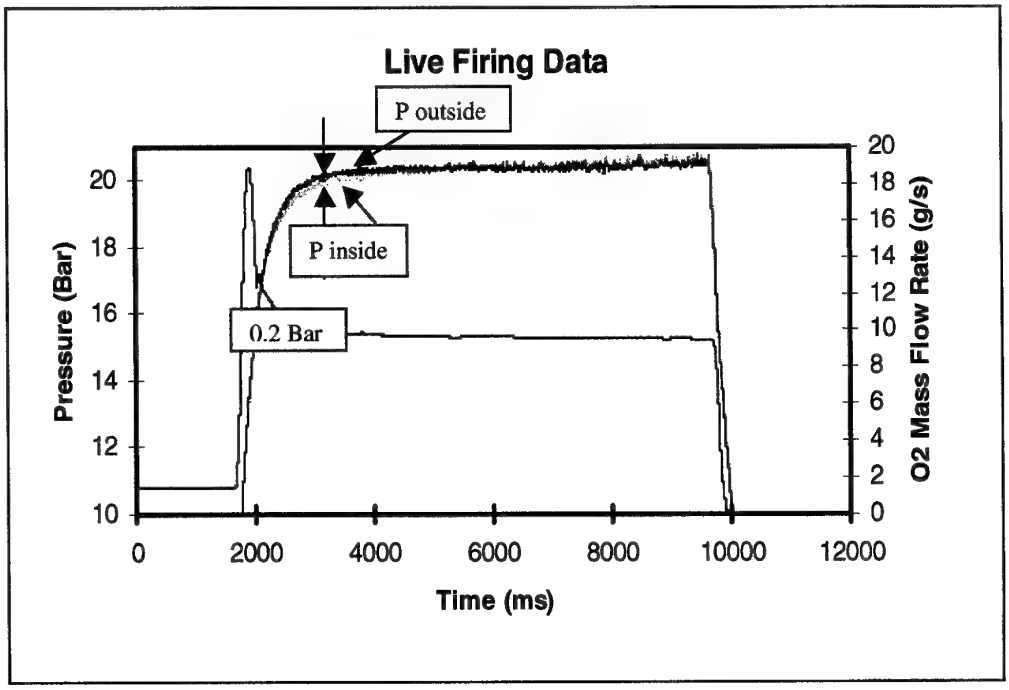

Chart 14. Diminished Pressure Gradient

The lack of a pressure gradient during hot firing and post firing analysis of the fuel grain suggest that the free vortex is not completing multiple revolutions around the engine during firing, rather that the boundary layers are

sufficiently slowing the free stream and exiting prior to a complete revolution. Figure 11 illustrates a sequence of photos taken though the PMMA fuel grain of the boundary layer flow during steady state firing. Note that the flow within the boundary layer completes approximately ½ a revolution prior to approaching the centrally located engine exit (the "free" vortex must be rotating further around than the boundary layer in order to influence the boundary layer in this manner). A weak vortex translates to a weak centripetal force within the combustion chamber, however, combustion efficiency measurements indicate the weakened centripetal force is still sufficient to enhance mixing of the fuel and oxidiser. A weak vortex has the added advantage that that it will have less of a tendency to "spin" the exhaust gases and thus create an attitude control (spin) problem for the spacecraft.

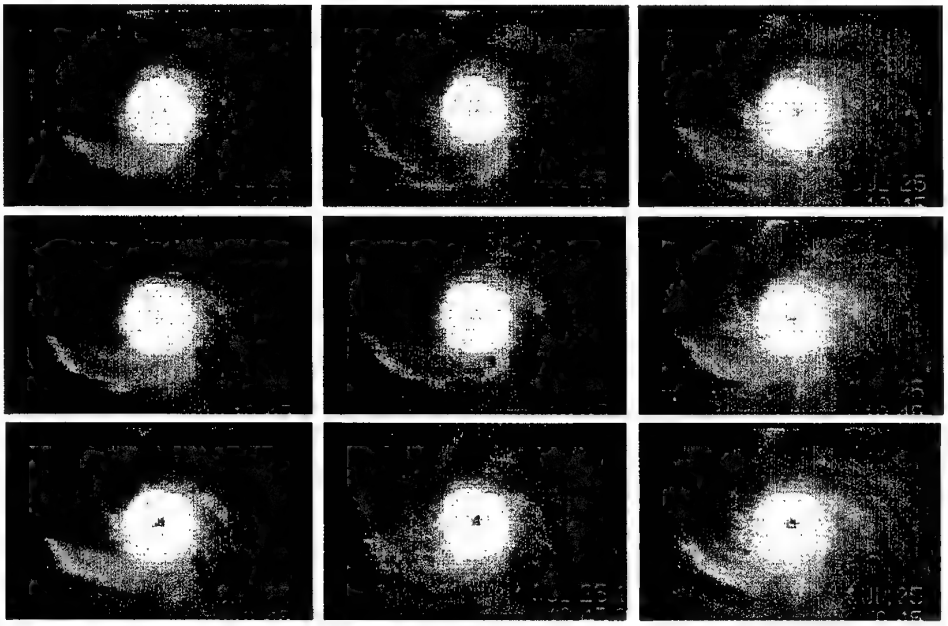

Figure 11. UV Filtered, Sequential Firing Photos During Steady State Firing

The VFP chamber pressure has been extraordinarily smooth over all regimes tested. The VFP engineering model regularly exhibited steady state combustion chamber pressure fluctuations of less than +/-1%. Smooth chamber pressure lends itself to more consistent operational characteristics (fuel vaporisation and thermal characteristics) and less vibration transmitted back to the spacecraft [Sutton 92].

4.4 Localised Fuel Liberation

Fuel liberation within the alternative geometry hybrid is more difficult to analyse than the conventional hybrid due to the fuel grain patterning effect. As the burn progresses the patterning effect becomes more pronounced. High injection velocities and fewer injectors enhance the effect, which results in an acceleration of the fuel mass flow rate from the solid grain. Figure 12 visually illustrates this effect.

Figure 12. Progressive fuel grain patterning representing a) 8 seconds, b) 16 seconds and c) 24 seconds at an injection velocity of 7m/s and O2 mass flow rate of 11g/s.

In addition to the grain patterning, the grains tend to preferentially regress at the periphery of the engine - especially at high injection velocities; this is attributed to the oxygen being injected at the periphery as well as the tendency of cool oxidiser to travel near the wall (injection momentum). Figure 13 illustrates this effect on a set of fuel grains from and early version of EM1; this set of fuel grains (top and bottom) was sectioned across the diameter of the grain illustrating preferential fuel liberation at the combustion chamber periphery (note: this grain did not employ boundary layer steps). These grains were subjected to high injection velocity (>70m/s) and high oxidiser mass flow rate for 10 seconds.

Figure 13. Preferential Fuel Liberation at Periphery

In contrast, fuel grains subject to lower injection velocities experience a much slower consumption of fuel at the periphery (and a slower overall patterning). Figure 14 illustrates the cross-sectional view of a fuel grain that was sectioned after accumulating 90 seconds of firing time; this grain was subject to a 7m/s injection velocity at 11 g/s; originally 25mm thick, the grain was consumed down to approximately 7mm thick.

Figure 14. Reduced fuel liberation with lower injection velocity and oxidiser mass flow rate.

4.5 Fuel Liberation Summary

Table 9 summarizes the trends identified during the fuel liberation parametric analysis. The positively identified trends relating to solid fuel liberation provide powerful tools to design for controlled fuel liberation within the new hybrid rocket design.

Given the facts that:

a) The combustion chamber flow field is non-axial and therefore difficult (if not impossible) to extract a meaningful mass flux metric.
b) Establishing a **lack of dependence** between fuel liberation and chamber height over the regimes tested (i.e. geometry measurements).

It was determined that a "regression rate" formula based upon mass flux and port geometry would not be appropriate (or possible) to fit the VFP. Recall the basic premise of the conventional hybrid regression rate equation is the fundamental relationship between the growth rate of the port cross sectional area (effect on port mass flux) and the ablation rate of fuel (perpendicular to the smooth fuel surface); since none of these relationships have been observed within the VFP the fuel liberation rate must be calculated based upon the size and the effects of other fuel liberation enhancing parameters (Injection Velocity, Oxidiser Mass Flow Rate, Number of injectors and Chamber Pressure) .

Metric	Relative Influence
Fuel Grain Patterning	Strong Influence
Oxidiser Mass Flow Rate	Strong Influence
Chamber Geometry Effects	No Influence Identified Over The Regimes Tested
Number of Injector Effects	Influence, aggravates fuel grain patterning
Oxidiser Injection Velocity	Strong Influence, also aggravates fuel grain patterning
Combustion Chamber Pressure	Strong Influence

Table 9. Summary of fuel flow study

For similar geometries, equations 4 and 5 are useful for determining an initial fuel liberation rate. The fuel grain patterning and subsequent increase in fuel mass flow rate, serve to shift the O/F curve *downward* over the duration of the burn (under constant oxidiser mass flow conditions); this is the opposite effect of conventional hybrid operations [Humble 95]. Chart 15 illustrates this effect by plotting VFP experimental data with a typical hybrid O/F shift (provide by [Humble 95]). Since the increasing fuel mass flow rate is tied to the rate at which the patterning appears, the effect can be minimised by lowering the local injection velocity and (perhaps) by slightly altering the injection geometry.

For most small spacecraft applications, VFP operations would be optimised at low fuel mass flow rates (i.e. low thrust), without any O/F shift; therefore, a design that employs multiple injectors, low oxidiser injection velocity and low chamber pressure would correspond to the lowest thrust scenario. These conditions would minimize the vortex patterning effect and result in the most consistent performance for small satellite applications.

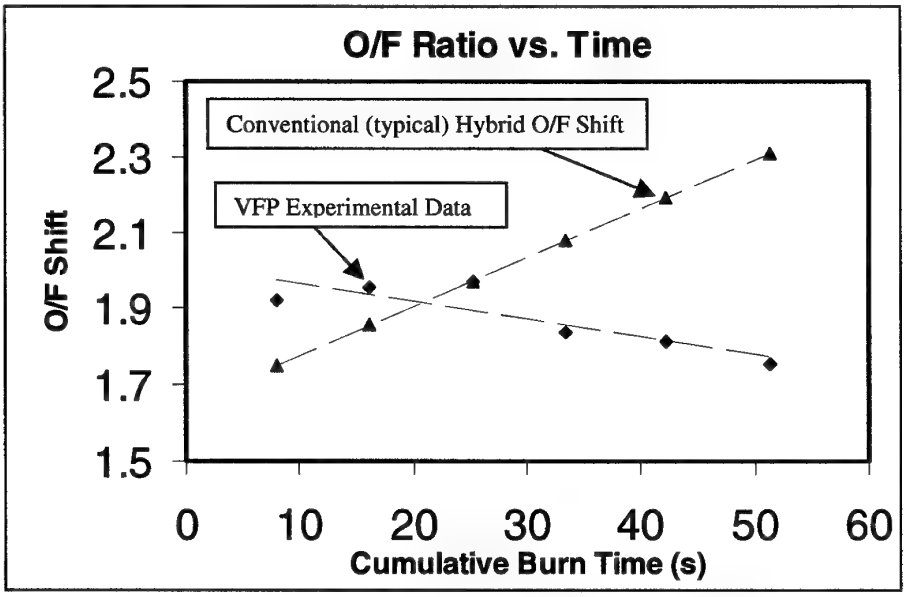

Chart 15. O/F Shift (VFP vs. Conventional Hybrid)

4.6 Engine scalability

Engine scalability was practically investigated by shrinking the combustion zone of EM1 and testing the configuration (while keeping other parameters constant). This was accomplished by employing thick stainless steel rings to shrink the diameter of the fuel grain (figure 15).

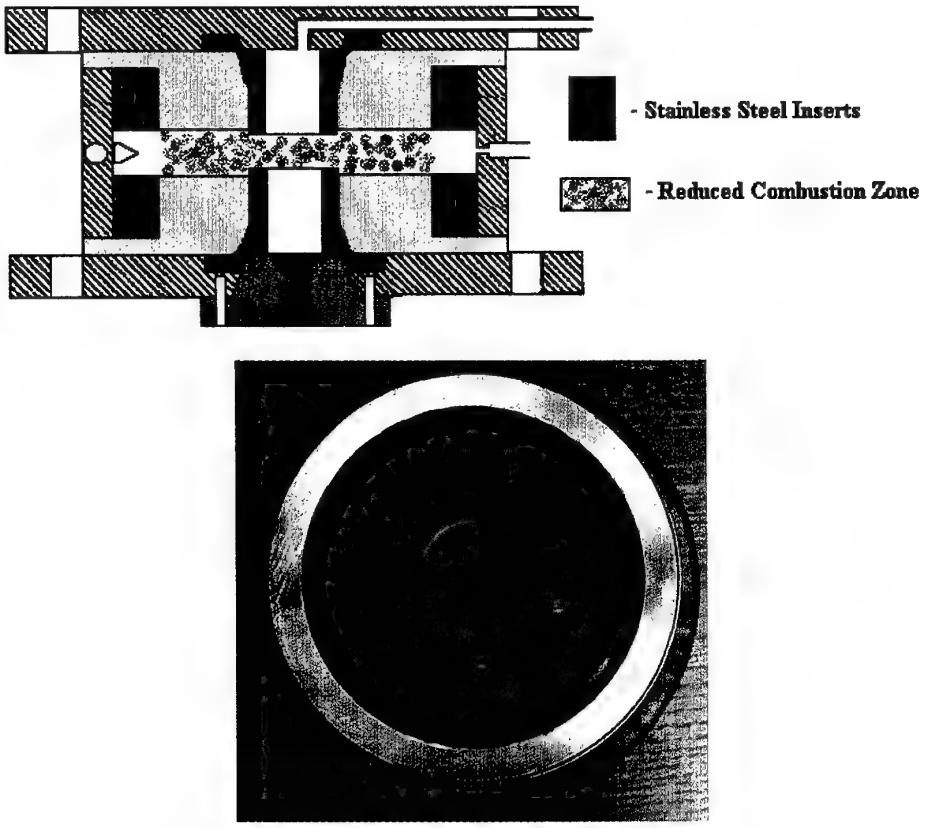

Figure 15. a) Cutaway view with 10mm thick fuel reduction ring
b) post firing fuel grain picture

Data were collected for fuel grain diameters of 121, 101 and 91mm. The 101 and 91mm configurations represented reductions of fuel grain surface area of 30 and 44% (respectively); every effort was made to keep other parameters constant, there was some low level variation in oxidiser mass flow rate, injection velocity, and combustion chamber pressure as outlined in table 10.

PARAMETER	OXIDISER MASS FLOW	INJECTION VELOCITY	CHAMBER PRESSURE
Avg. Variation	0.5 g/s	1.73m/s	1.6 bar

Table 10. Maximum variation witnessed during engine scalability testing

The primary purpose of this experimental investigation was to see if the there was any loss in combustion efficiency associated with a smaller combustion zone and to see that fuel liberation tracked fuel grain burn surface area. Similar to the other VFP combustion efficiency measurements, the efficiency figures were within 5% of theoretical during the engine scalability testing campaign. Chart 16 illustrates the near linear relationship between the fuel mass flow rate and fuel burn surface area, each data point represents the averaged fuel mass flow from 4 consecutive firings (a total of 12 firings). Here too, we see the effect from the vortex patterning[3] (skewing the linear relationship from the origin of the chart).

[3] Although other parameters have changed as well (distance between grain and injectors, subtle aerodynamic effects, etc.).

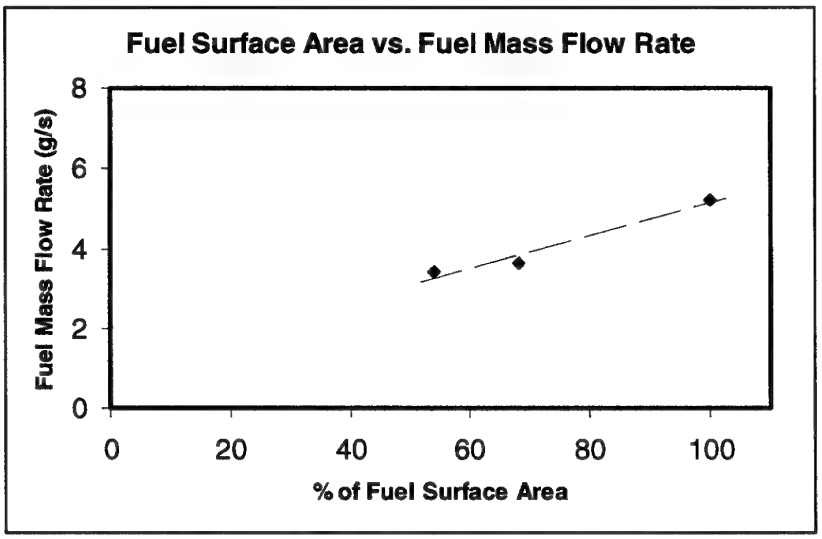

Chart 16. Engine Scalability Results

The scalability results are promising in that they indicate there is not a fundamental efficiency loss as the engine is scaled down. Small diameter chambers result in lower fuel mass flow rates and subsequently, lower (stoichiometric) thrust levels (chart 17). However, the potentially attractive attributes of shrinking engine diameter must be weighed against overall fuel loading in the combustion chamber and the tendency to "elongate" the VFP geometry.

An expression for fuel liberation was developed for the fuel surface area as well; it should be noted that the relationship has only be tested over engine radii from .0455 to .0605m.

$$Mf = 120.166\ (InVel)^{.2832}\ (r)^{1.3504} \qquad \text{(Equation 6)}$$

Where:
Mf – Fuel Mass Flow Rate (g/s)
InVel – Oxidiser Injection Velocity (m/s)
r – Engine radius (m)

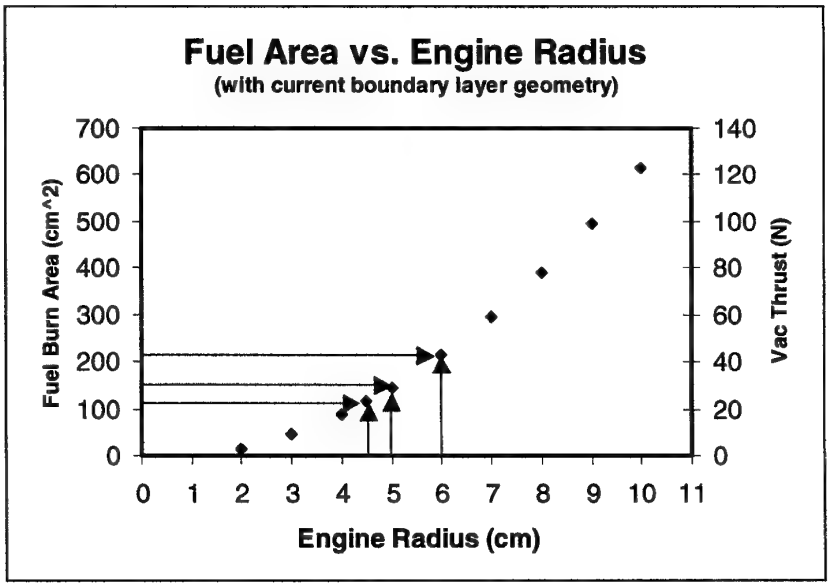

Chart 17. Engine Radius vs. Fuel Area and Vac Thrust

4.7 Flight Propellant Testing

VFP operations were also conducted with N2O and HTP. N2O and HTP, like all flight propellants, are energetic substances and every energetic substance has the potential to be dangerous. However, in the overall scheme of rocket propellants both N2O and HTP are considered relatively safe. In addition, both propellants can be classified as "green propellants" because they do not represent a credible danger to the environment. If spilled, HTP readily decomposes to water and oxygen. N2O, while considered a potential "green house gas" is of no threat to the environment for two specific reasons. First, when exposed to the heat of combustion, N2O decomposes into nitrogen and oxygen (major constituents of the atmosphere). Secondly, accidental releases associated with research, development, test and operations of N2O based spacecraft propulsion systems would be negligible compared with the amount of N2O generated daily by cars, factories, the medical industry and natural sources.

All N2O ops were conducted within the EM1 test engine while HTP operations spanned both EM1 and EM2 engines. N2O stores as a liquefied gas while HTP stores as a liquid, they have a specific gravity of ~0.75 and 1.4 (respectively). While N2O does not store as densely as HTP, it does have the added benefit of being self-pressurised (vapour pressure of approximately 50 Bar at 20°C), possibly eliminating the need for separate pressurisation system. A N2O oxidised hybrid would also have an inherent capability for a multi-mode (cold gas, resistojet, or monopropellant) propulsion operations. However, in order to retain the highly desirable re-start capability of the hybrid, the N2O hybrid would require the development of a ignition device that would allow multiple restarts of the hybrid engine over the span of its operational life. In addition, the N2O propellant tank will have to be designed stronger (i.e. heavier) than the HTP equivalent tank.

HTP stores almost twice as compactly as N2O and has a reliable, easily achievable ignition mechanism (catalytic decomposition of the HTP). The HTP however, must be pressurised by some means, requiring a pressurisation/expulsion system. HTP also auto-decomposes, slowly building up pressure in a sealed vessel; this characteristic must be considered in the propulsion system design and operations concept for any HTP based system.

4.7.1 N2O TESTING

N2O testing began on the EM1 by passing gaseous N2O into the combustion chamber and igniting the engine with a hot wire (similar to gaseous oxygen operations). However, as the liquid evaporated within the N2O tank the tank temperature dropped rapidly. Subsequently, the ullage pressure and mass flow rate of oxidiser also decreased (chart 18). (Note: Tank pressure/mass flow recovery is not a fast as indicated in chart 18, the mass flow curves were artificially graphed together to illustrate the steady drop in oxidiser mass flow rate). While combustion proved to be smooth and steady, gas feed of the oxidiser would not be practical without providing significant energy to heat (and evaporate) the oxidiser within the tank (not a practical option for small, power hungry spacecraft).

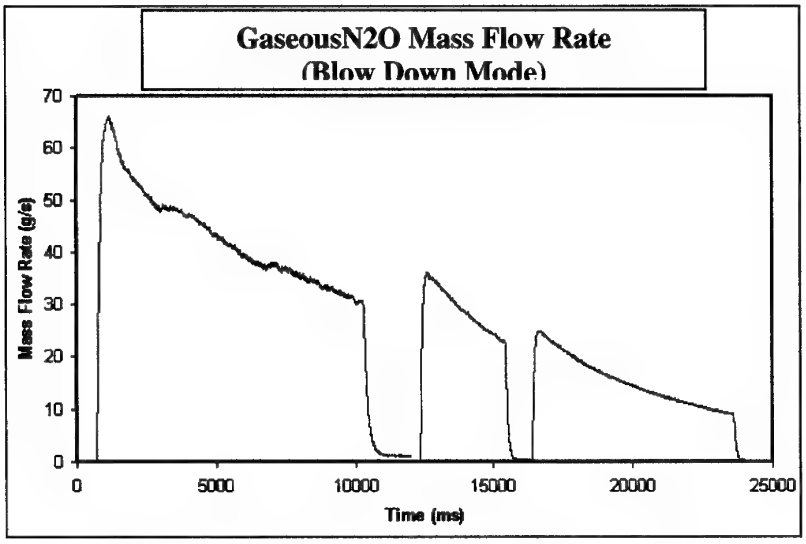

Chart 18. N2O Mass Flow Rate in "Blow Down Mode"

Liquid N2O feed of the VFP was attempted by using the ullage pressure of the N2O to push the liquid from the tank, through the flow meter, through the firing valve and into the engine. Once again, thermodynamics prevailed, as the volumetric flow out of the tank was immediately replaced by cold evaporating N2O gas, the tank temperature, feed pressure and mass flow rate dropped off. The only method found to effectively feed liquid N2O at the required flow rates (~50g/s) was by forcing the liquid from the storage tank with pressured gas (N2).

Initially, a choke valve was employed upstream of the firing valve in order to isolate the feed system from any combustion pressure feedback and facilitate vaporisation of the liquid N2O. This modification to the feed system proved fruitless as the extremely cold oxidiser hampered valve operation with the external build up of ice. The second modification was to move the choke to the injectors themselves. The N2O injectors were modified to employed brass chokes, providing a pressure drop across the 4 injectors. The pressure drop acted to isolate the feed system from any combustion pressure feedback and vaporise the liquid N2O as it entered the combustion chamber. This modification worked better but it presented two problems: First, it drew out the whole shutdown process as liquid N2O between the firing valve and the injectors would boil-off after closing the firing valve (chart 19 – note how pressure and thrust remain high after the oxidiser supply is cut off). Secondly, as the vaporised N2O left the injector head, it sprayed a mixture of minus 50°C two-phase (gaseous and liquid) N2O onto the fuel grains cooling the whole engine assembly and covering the engine in frost (figure 16). The oxidiser cooling was so intense that it froze the cooling water in the rocket nozzle prior to ignition. In order for a hybrid engine to operate, the fuel must be vaporised from solid form in order to feed the combustion process, the freezing oxidiser inhibited the hybrid process by keeping a large majority of the fuel locked up in solid form.

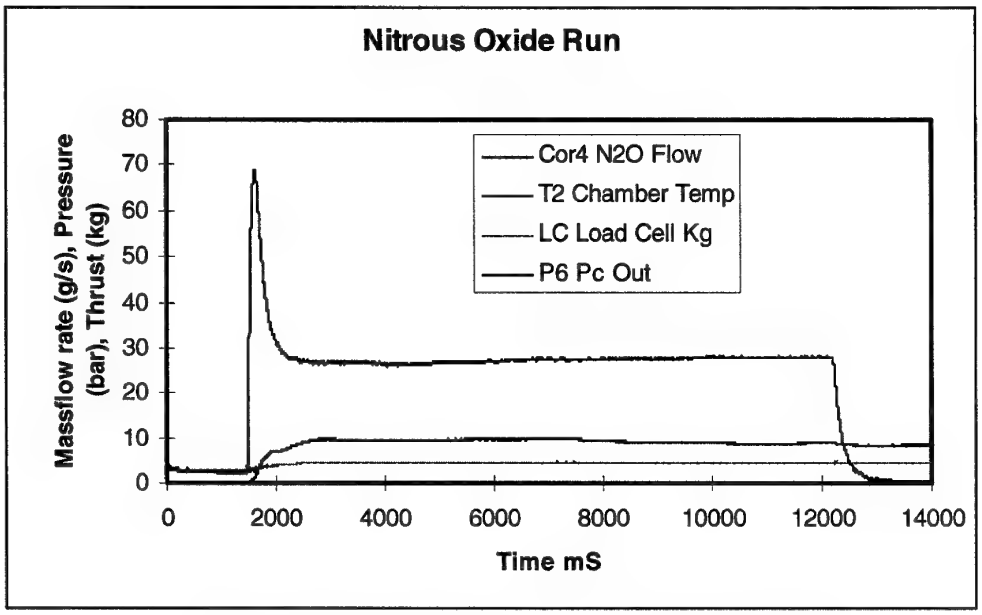

Chart 19. Nitrous oxide run with chokes at the injector

EM1 was designed to operate with gaseous oxygen and PMMA. The fuel grain size was based around a nominal thrust of 35N with an O/F of 1.3, thus, to push the O/F up for N2O/PMMA (to approximately 9) while maintaining thrust to less than 200N, a smaller fuel grain geometry was needed. Borrowing from the engine scalability test apparatus (section 4.6), it was felt that the stainless steel inserts would provide a cost effective method to reduce the size of the fuel grains and thereby improve the mixture ratio (without pushing engine thrust above a 200N threshold). The stainless steel inserts effectively reduced the size of the fuel grains but inadvertently created a circular raceway (an area not exposed to the burning fuel surface), for a mixture a gas and liquid oxidiser to pool (while circulating) around the periphery of the engine. The liquid N2O firings were notoriously difficult to ignite with the hot ignition wire. Once ignition was achieved, only a small portion of the fuel grain under the ignitor (the "ignitor burn area") actually ignited because the cold oxidiser was keeping the fuel locked in solid form (figure 17). Combining this scenario with the centripetal forces within the engine (casting any vaporised, unburned fuel outward) caused a large pressure excursion – relieving the gaskets in the test assembly (as designed) but damaging the EM1 hardware, pressure transmitters and the load cell (Chart 20). At this point, a decision (based on safety) was made to halt N2O testing.

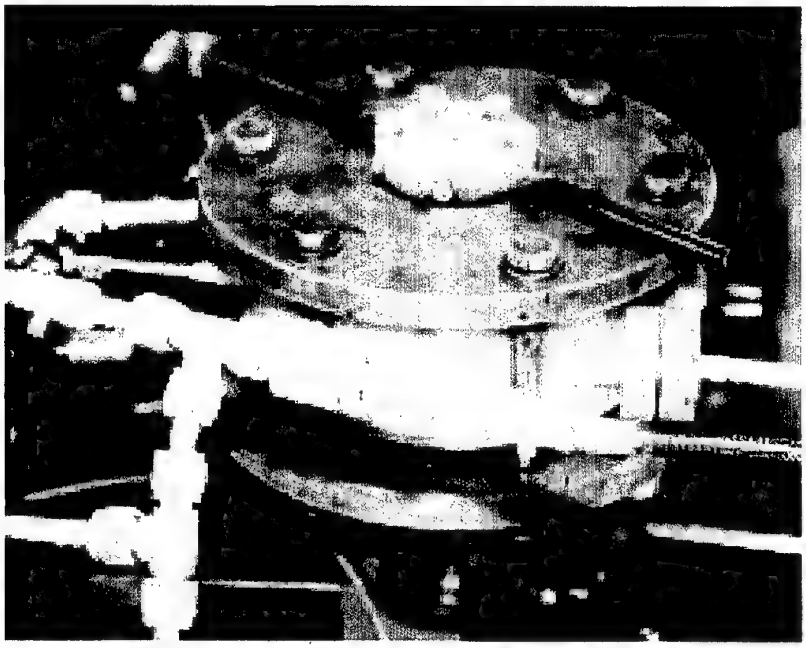

Figure 16. Frost from liquid N2O Evaporation

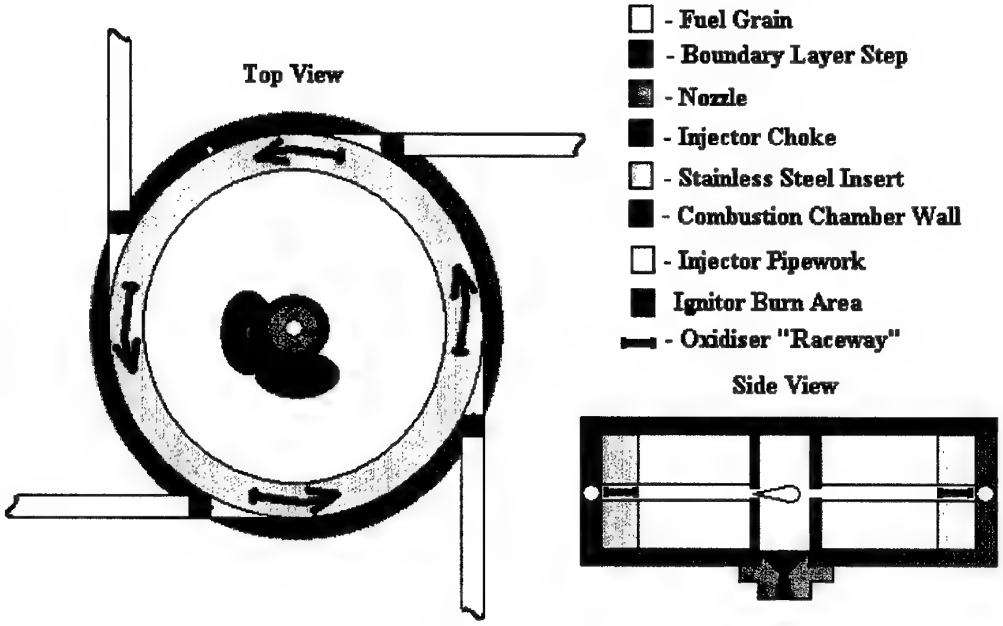

Figure 17. N2O injection configuration

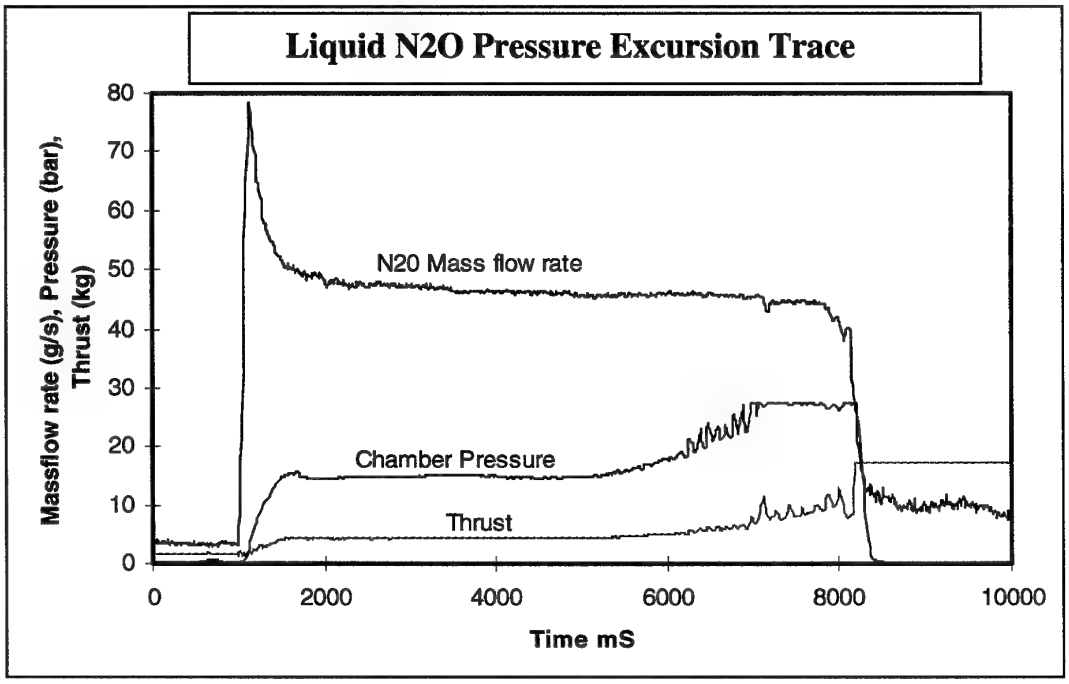

Chart 20. N_2O Pressure Excursion

Although the engine configuration could be made completely safe to operate with liquid N2O by:

1. Increasing the number of injectors and pressure drop across the injectors (thus avoid two phase injection of N2O).
2. Keeping the fuel burn surface area adjacent to the chamber wall (reduce the capacity of the configuration to pool oxidiser).
3. Employ a more energetic ignition device (to ensure both fuel grains are completely ignited).

The VFP research program was running out of time (and funding) to implement the changes. In addition, N2O operations appeared to require the addition of a pressurization system to support the high flow rates necessary for hybrid operation, thus the attraction of N2O as a space flight hybrid oxidizer was significantly reduced[3]. Subsequent testing with a fellow researcher found the practical limit for N2O flow rate (using the vapour pressure to expel liquid) to be less than 10g/s. [Zakirov 01]. The remaining flight propellant practical research was devoted to operations with high test peroxide (HTP).

4.7.2 HTP TESTING

HTP operations were conducted on both EM1 and EM2, however, EM1 HTP testing was always extremely fuel rich due to the high O/F required for stochiometric HTP/Polyethylene (PE) operations and the amount of fuel available (fuel grain surface area). EM2 eased the fuel abundance problem by reducing the overall surface area of exposed fuel to combustion (32% reduction in available fuel area). Black PE was chosen over both white PE, PMMA and HTPB for two reasons; first, PE burns much cleaner than PMMA, and HTPB (no soot), an important consideration for spacecraft with optics or other contamination sensitive payloads. Secondly, the black PE blocks the thermal radiation from penetrating deep into the solid fuel grain, thus helping to minimise fuel liberation. Chart 21 illustrates a high pressure (~30 Bar) EM2 firing with Black PE and HTP. During this firing, ignition occurred within 0.54 seconds of initiation of HTP flow. Note the chamber wall temperature stabilises at approx 630°C as a result of the (relatively) cool HTP decomposition products being sprayed on the wall. Chamber pressure and thrust are exceptionally steady and smooth for the duration of the ten-second run.

[3] N2O has a density approximately ½ that of HTP (.75 g/cm3 vs. 1.4 g/cm3). The ability to self pressurize and feed the hybrid (thus avoid a separate pressurization system) was overestimated. If a separate pressurization system is necessary, HTP becomes a much more attractive propellant due to a higher density specific impulse.

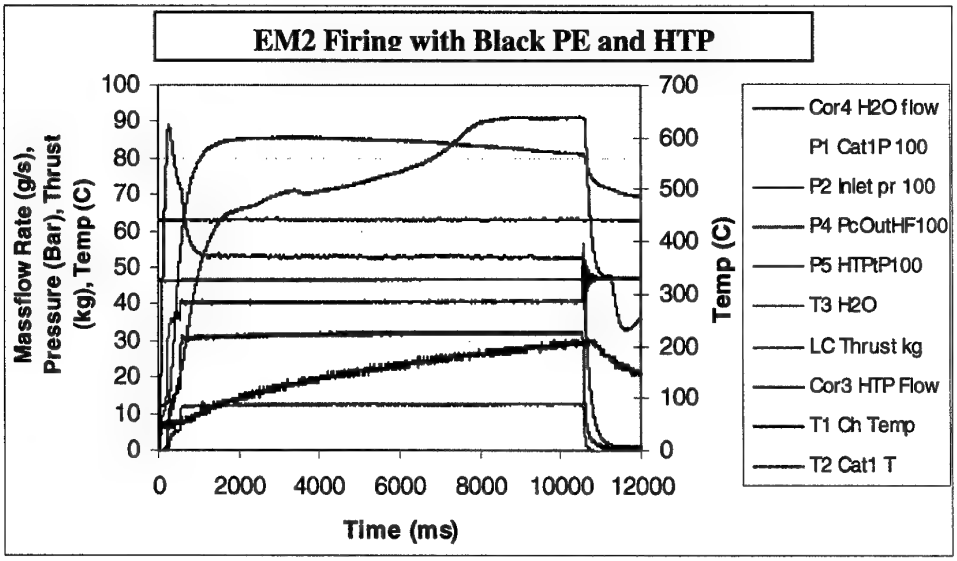

Chart 21. HTP Firing Trace

Similar to Gox/PMMA operations, the combustion efficiency of the HTP/PE firings was very high. Twenty-seven HTP firings were conducted while collecting characteristic exhaust velocity measurements (chart 22). The combustion efficiency from these firings averaged 96% of theoretical performance (theoretical performance being calculated with the Isp computer program [Selph 92]); Fourteen HTP firings yielded thrust measurements and subsequent Isp values averaging 95% of theoretical (chart 23). However, it should be noted that the HTP figures have a considerable more amount of error than the Gox/PMMA measurements due to the catalytic auto ignition scheme employed.

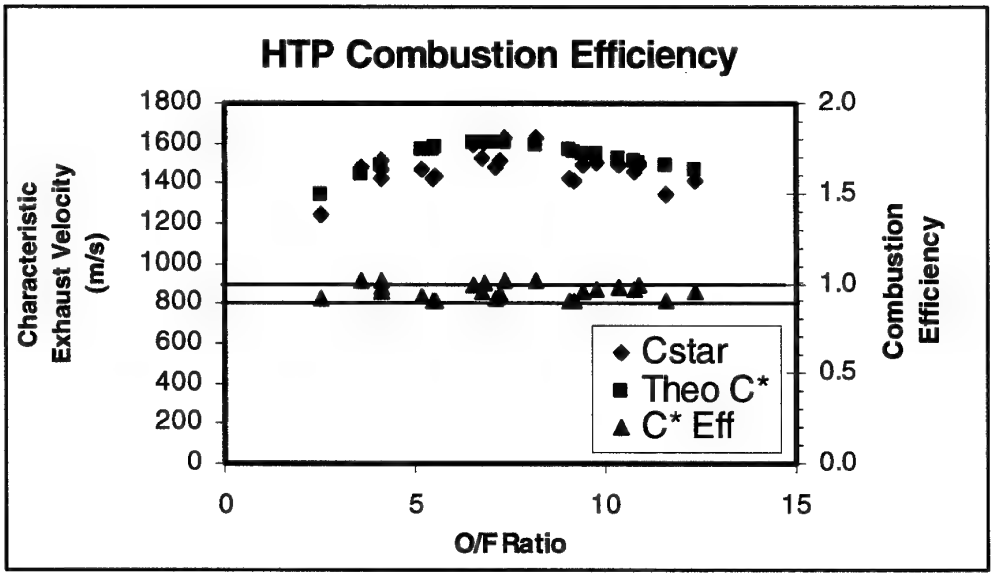

Chart 22. HTP Combustion Efficiency

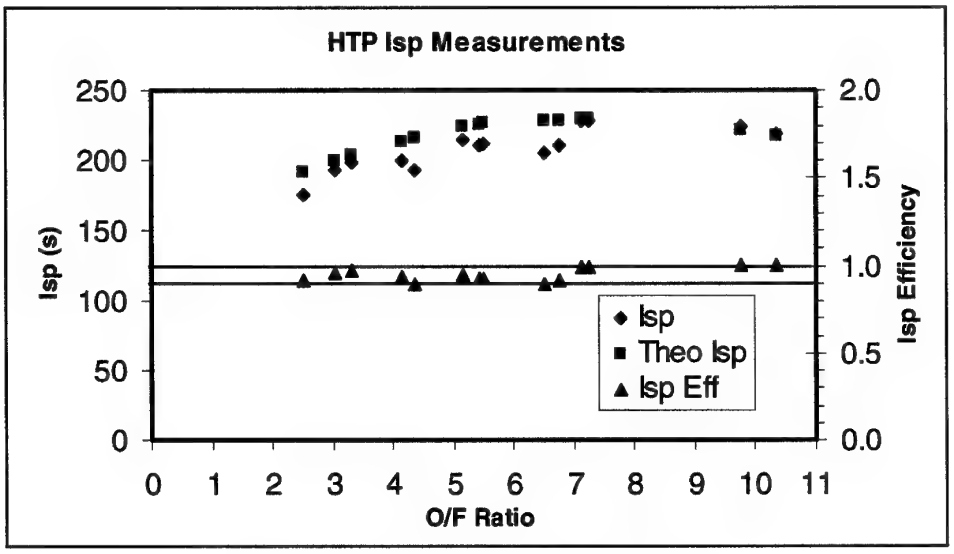

Chart 23. Isp Measurements for HTP/PE

Catalyst induced auto-ignition is achieved by injecting high pressure HTP through a bed of tightly packed silver screens, once in contact with the silver, the HTP exothermically decomposes into superheated water vapour and oxygen. The superheated steam and oxygen are then injected into the combustion chamber were the residual heat vaporizes some of the solid fuel grain and if hot enough, ignites the engine. Theoretical decomposition temperatures for 89% peroxide approach 740°C [McCormick 65], however, the efficiency of the catalyst pack and thermal losses in the system determine how much time expires before ignition occurs. Since fuel mass flow rate is determined by pre and post firing weight measurements, any fuel vaporization that occurs prior to ignition induces errors in the fuel mass flow rate calculation. In addition to the thermal characteristics of the engine, catalyst pack lifetime and poisoning also affected the start-up duration. Start-up delays as short as 0.2 seconds and as long as 8.0 seconds were recorded, however, only runs with start-up durations of less than 2.5 seconds were considered accurate enough for comparison.

As mentioned in Chapter 5, EM2 was purposely elongated in order to facilitate exaggerated fuel loading scenarios and chamber geometry measurements (figure 17). Unfortunately, the long chamber design exasperated the ignition delay when chamber geometry measurements were conducted because the large amount of chamber wall exposed to the incoming decomposition products robbed heat (i.e. ignition energy) from the hot oxidiser. However, once ignited, the engine provided smooth and stable combustion over all levels of fuel utilization tested.

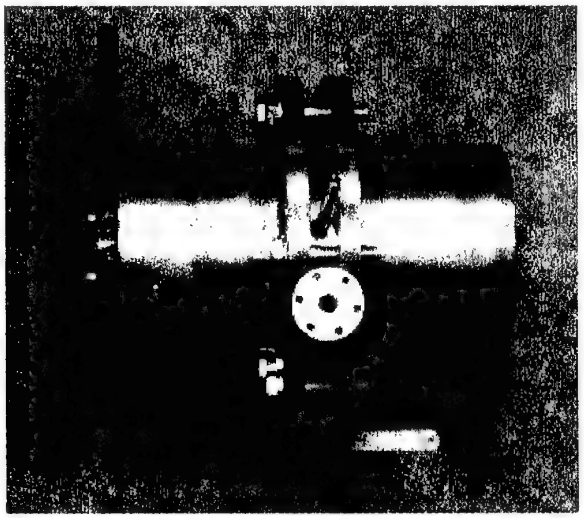

Figure 17. EM2 (side view)

Another interesting aspect of the EM2 test campaign was firing only half the engine. In order to address lower fuel mass flow rates and thrust, one half of the engine was blanked off with a stainless steel flange while the remaining fuel grain was fired (figure 18). Two runs with this configuration yielded very high combustion efficiency at approximately the 85N thrust level (Table 6.13).

Run	O/F	Cstar	Pc	Mf	Thrust	Isp	Isp Eff	C* Eff
1	6.75	1531	22.34	5.56	89.25	211	0.92	0.95
2	6.85	1611	21.22	4.98	81.88	214	0.93	1.00

Table 11. EM2 Single Fuel Grain Firing

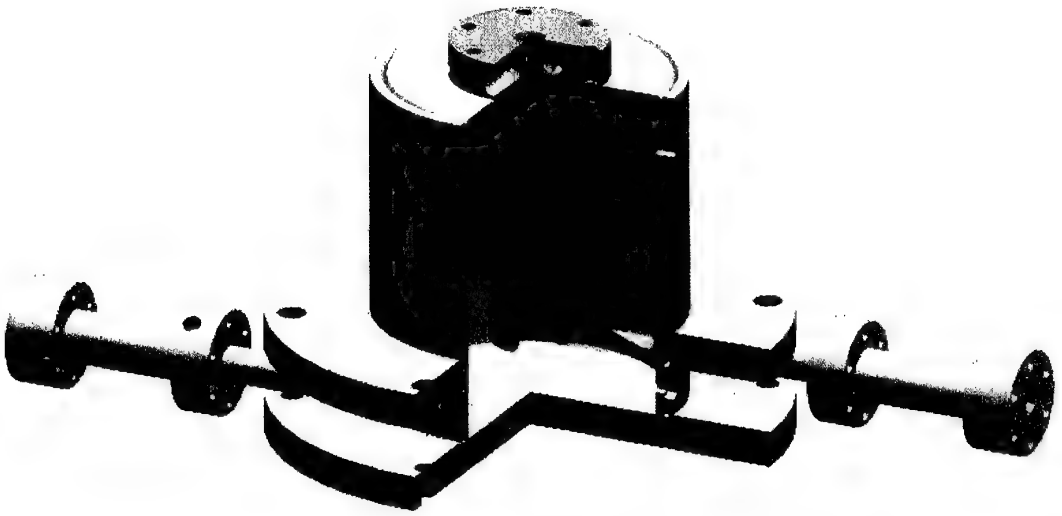

Figure 18. EM2 Reduced Fuel Area Configuration

The HTP/PE test campaign validated some of the previous findings from the Gox/PMMA testing. First, the VFP produces high performance with the flight propellants; C* and Isp measurements were correspondingly high and combustion was remarkably smooth. Second, as demonstrated by the Gox/PMMA firings (covered in section 4.8), the chamber wall film cooling appears to work well with HTP decomposition products, indicating inexpensive materials can be used to construct a flight engine. While new fuel grains (near the HTP injectors) exhibited the vortex patterning effect and characteristics similar to EM1, grains positioned further away (>6cm from the injectors) had difficulty igniting as the stainless steel combustion chamber wall would absorb ignition energy from the hot oxidiser stream.

Chart 21 illustrates a Fast Fourier Transform of EM2 combustion chamber pressure. The primary emphasis of this chart is to illustrate the (low) magnitude of the chamber pressure amplitude. Waveforms under 500 Hz are attributed to mechanical inputs such feed lines and valves while the higher frequency waveforms are attributed to acoustic sources such as the interface between the combustion chamber wall and the HTP inlets, the interface between the pressure tap and the combustion chamber wall, etc.

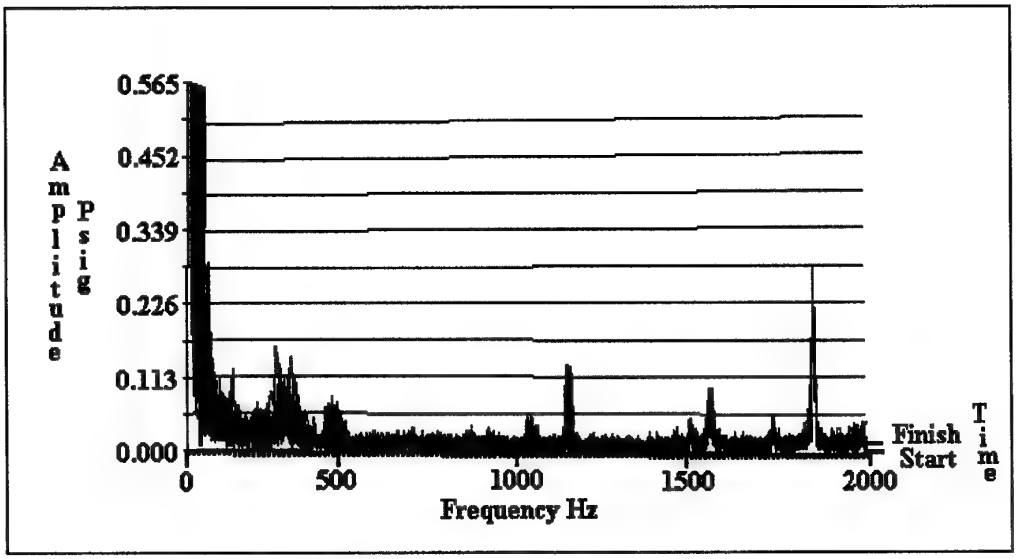

Chart 21. High Frequency FFT of EM2 with HTP and PE

4.8 Other Findings

Long duration firing

VFP firings were nominally kept under 10 seconds in order to preserve the pyrolytically coated carbon boundary layer steps. Ordinarily, EM1 boundary steps would last for approximately 5 fuel grain sets (with an average of 8, eight second firings) before their height would erode below the level of a new fuel grain set. Long duration burns eroded the steps much faster so this condition was avoided. However, on one occasion, the engine was configured and fired for a continuous 45 seconds. The primary purpose of this test was to allow the nozzle cooling water to reach a steady state operating temperature (to allow for calculation of the energy being taken out by the water cooled nozzle arrangement). Chart 24 presents the raw (unprocessed) firing trace; note how the injected oxidiser effectively cools the chamber wall. Although the boundary layers were damaged (eroded) during this run, the fuel "erosion" occurs more quickly, preserving a boundary layer trip for the life of the fuel grain set.

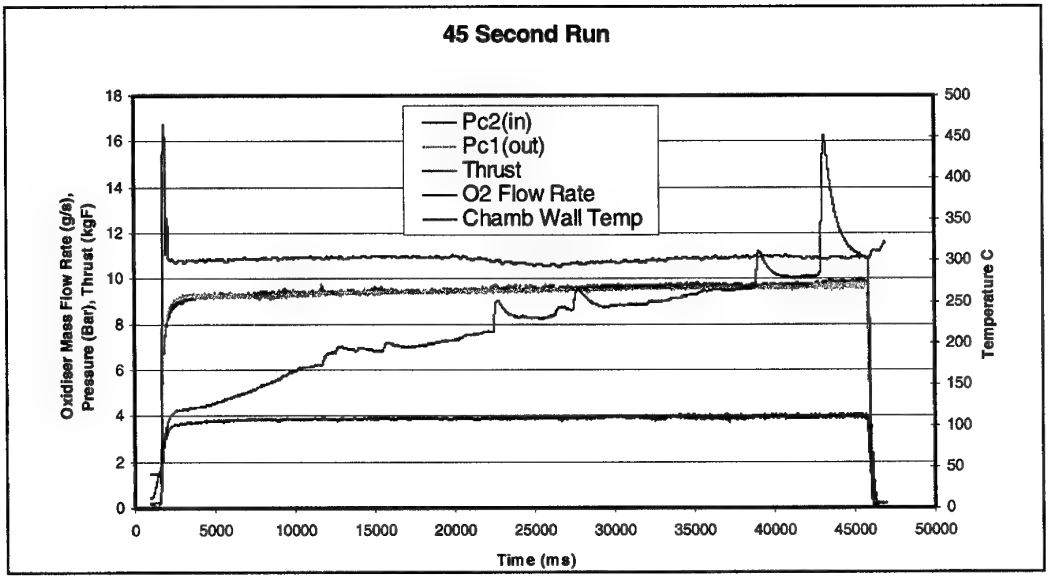

Chart 24. Long Duration (45s) Firing

Pulsed Operations

In order to establish the reproducibility of the engines operating characteristics, a test demonstrating pulsed operation was conceived to demonstrate how reliably the engine would return to steady state conditions. The test was not representative of any particular operational mode as it used the residual heat of the combustion chamber for ignition while the oxidiser flow was cycled on and off. Chart 25 illustrates 14 consecutive relights, demonstrating remarkable uniformity of operations (returning to within 1.5% of steady state operational values for chamber pressure and thrust).

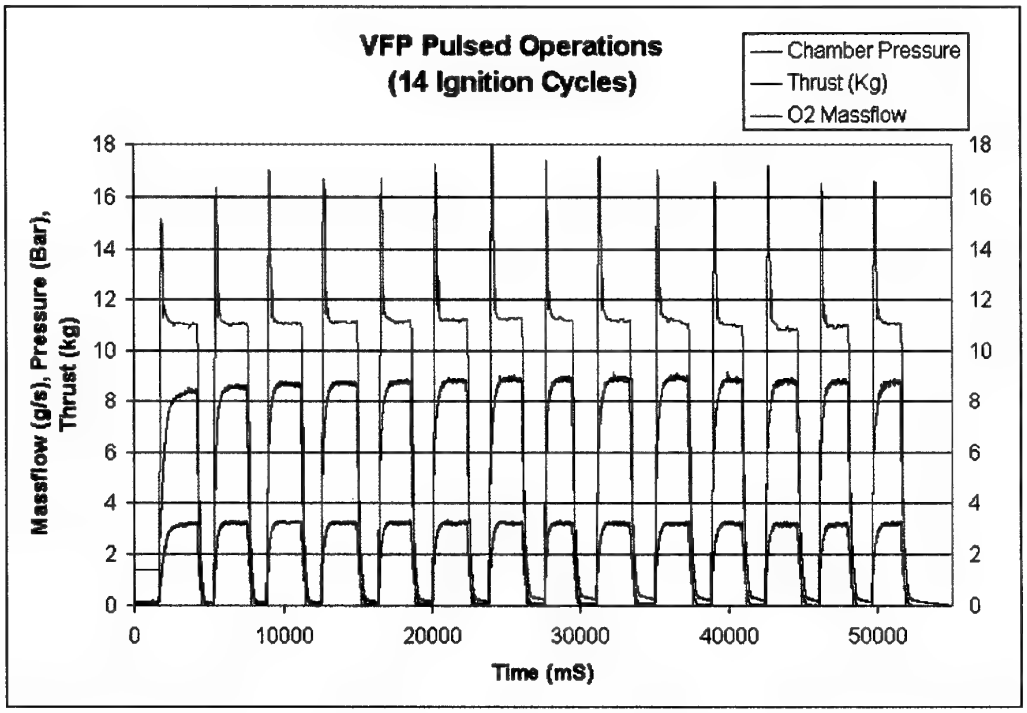

Chart 25. Repeatable Performance Demonstration

Thermal Measurements

The thermal benefits of the VFP are the ability to mount all the hot components of the rocket engine external to the spacecraft and the inherent film cooling mechanism within the combustion chamber. It was expected that the VFP would get good chamber cooling effects from the centripetal acceleration (gas separation) within the vortex and the oxidiser film cooling effect on the combustion chamber wall. By extending a thermocouple through the combustion chamber wall, temperatures just inside the wall were measured (figure 19). With a thermocouple located at a depth of 1 mm into the combustion chamber, the engine was fired 29 times (6 second durations) delivering temperatures of less than 180°C on all but 1 run (when temperature reached 600°C), chart 26; this anomalous temperature was most likely due to a piece of fuel or engine sealant that had broken loose and burned on the thermocouple during this run. Extending the thermocouple 5mm into the combustion chamber (for 8 runs) resulted in temperatures routinely reaching 500°C and higher (the thermocouple was destroyed on the 8th run as temperature climbed through 900°C), chart 27.

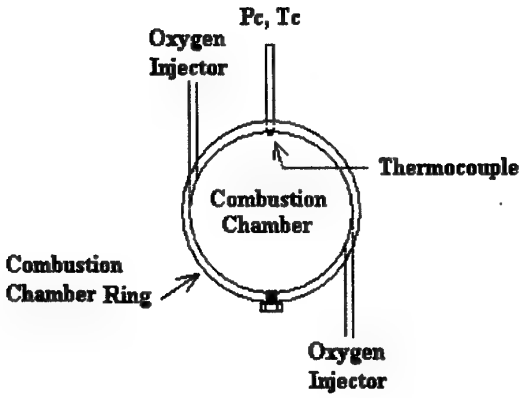

Figure 19. Chamber wall thermocouple location

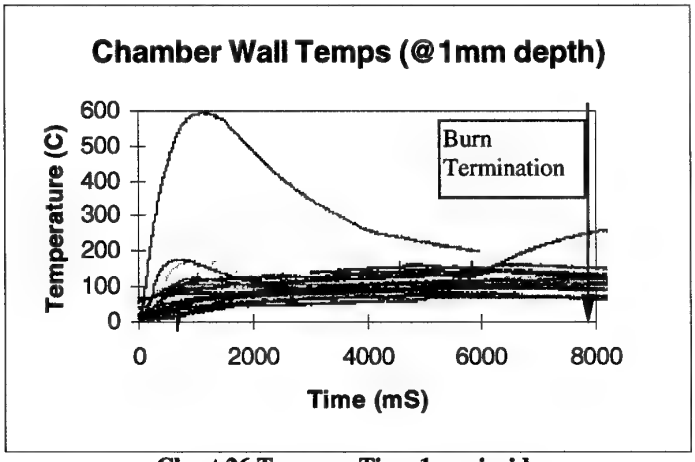

Chart 26 Temp vs. Time 1mm inside the VFP combustion chamber

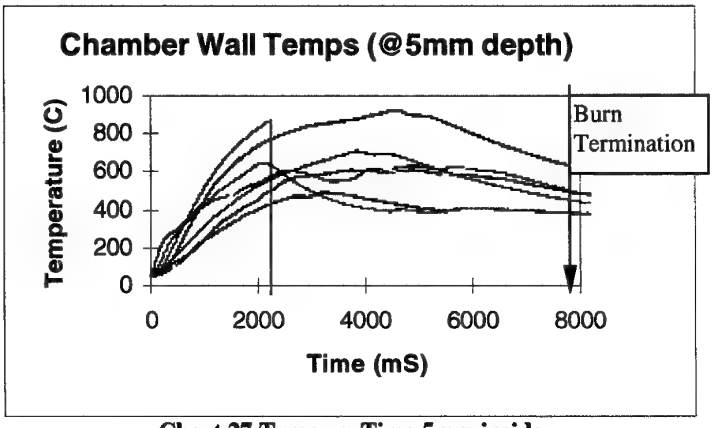

Chart 27 Temp vs. Time 5mm inside the VFP combustion chamber

Nozzle Blockage Mitigation

It was theorised that the centripetal acceleration within the VFP would keep solid particulate (such a solid fuel slivers) from approaching and potentially blocking the nozzle. The risk of fuel slivering and nozzle blockage within the conventional hybrid necessitates leaving unburned fuel within the combustion chamber; by reducing or eliminating the risk of nozzle blockage the VFP could use more fuel or possibly be burned to completion. Although there hasn't been any specific "fuel sliver" experiments conducted within the VFP, there is evidence that the forces within the engine keep solid particulate from approaching the nozzle; occasionally, the silicon sealant used to seal the surface between the fuel grains and combustion chamber wall frothed into solid stone-like objects. After such a firing, small particles of the stone-like objects would be distributed around the perimeter of the combustion chamber. On one occasion, a large silicon "rock" was filmed circulating around the chamber in a polygonal path colliding with the wall of the engine as the oxidiser flow subsided (figure 20). It is anticipated that any slivered fuel would continue to circulate within the vortex flow-field until it was fully consumed by combustion or smashed to bits by collision with the wall in true vortex mill fashion [UoH 99] .

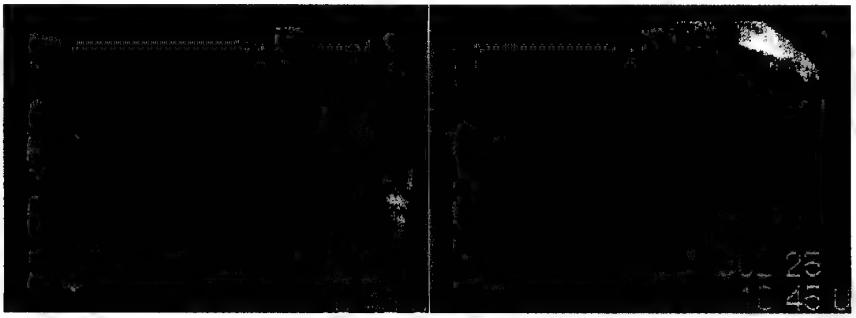

Figure 20. Solid particulate travelling along the chamber wall

Angular Momentum

Tangential injection of the oxidiser into the combustion chamber will impart some angular momentum into the spacecraft if the rocket exhaust leaves the engine with a spin. Since the VFP was envisioned to be operated in conjunction with a spinning spacecraft, any slight disturbances of the spin vector caused by VFP operation could be easily absorbed by the mission spin up/down budget. However, non-spinning operations would be advantageous as well. Therefore the magnitude of momentum imparted was investigated.

Momentum can be imparted into the spacecraft by exhaust gases carrying some of the vortex spin divergently out of the rocket nozzle. Divergent flow out the nozzle would be a serious problem because the nozzle would be inefficiently using some of the rocket propellant to spin the spacecraft. This unwanted characteristic, if present, would have to be identified and minimised.

The primary mechanism used to determine if spinning flow was exiting through the nozzle was C* measurements with a standard configuration in comparison with a configuration that blocked the spinning flow from exiting the nozzle. C* provides a ratio of pressure achieved for a given propellant mass flow rate and throat area. For one-dimensional flows, C* is a straightforward measurement. However, research [Goldman 96] has indicated that swirling flows alter the effective area of the nozzle throat; in essence, large swirl velocities would impose a *vena contracta* within the nozzle that would manifest itself as a higher chamber pressure for an apparent nozzle area. In other words, if the VFP had a large swirl velocity exiting through the nozzle, the chamber pressure (and C*) would be higher than for non-swirling conditions. Therefore, an experiment was conducted to provide straight flow through the rocket nozzle.

In order to ensure the flow entering the nozzle did not have a swirl, a modified copper boundary layer step was employed. Boundary layer steps are employed within the VFP to reintroduce fuel that is trapped within the boundary layer to the mixing action of vortex flow field. The modified boundary layer step incorporated a flow straightener that prevented swirling flow from entering into the nozzle (figure 21). This configuration did however limit burn duration's to three seconds or the boundary layer step would begin to melt. Test results demonstrated that C* values were not appreciably effected by exhaust gas swirling through the nozzle (chart 28).

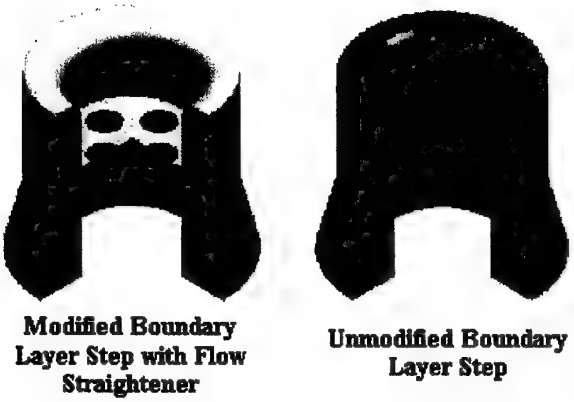

Figure 21. Boundary Layer Steps

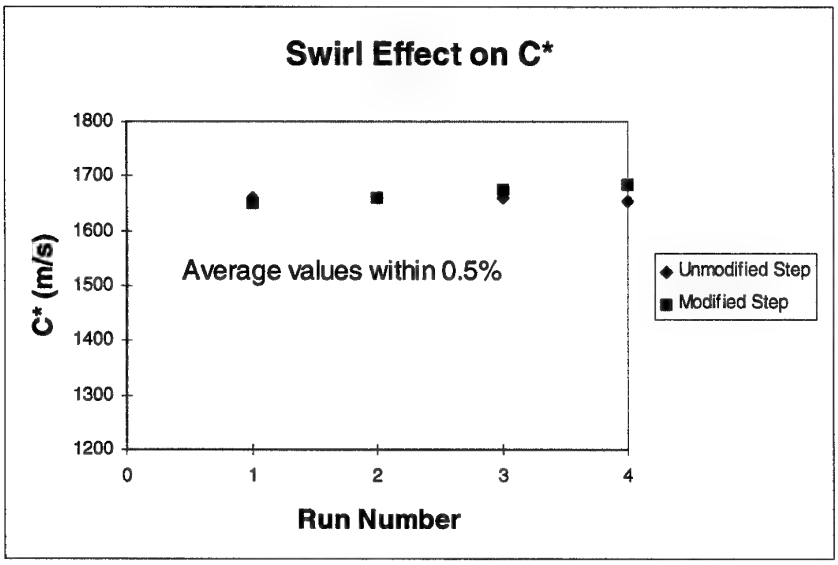

Chart 28. Swirl vs. Non-Swirl Investigation

Fortunately, this research program is interested in low thrust and subsequently, low oxidiser injection velocities. A low oxidiser injection velocity minimises the potential for adverse ACS effects from spinning exhaust gases. In addition to monitoring the rocket exhaust plume for signs of divergent flow (presence of swirling steam or smoke) the VFP had been fired with cold gas on an air bearing table (capable of discerning 1mNM of torque), these cold gas 'firings' of 800 PSI N2 did not cause any discernable torque during operation (figure 22).

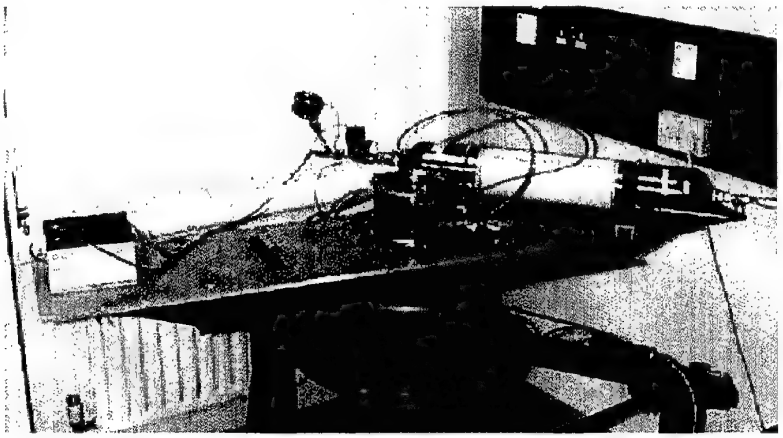

Figure 22. Torque measurement on an air-bearing table.

N2O Auto-ignition

Although N2O operations of the VFP were not reliably demonstrated in this program, one novel achievement was made with respect to N2O operations. HTP can be decomposed over a catalyst bed in order to achieve reliable ignition, it was assumed that N2O operations would require some type of pyrotechnic device in order to achieve rocket engine ignition; cooperation with a fellow SSC propulsion research program [Zakirov 00] whose research specialty was catalytic decomposition of N2O, led to a successful demonstration of catalytic N2O auto-ignition of the VFP. The test used an external heat source to heat two catalyst beds of Shell 405 to a temperature of 250°C then applied a low flow of N2O gas through the catpacks. The catalyst effectively lowered the decomposition temperature of the N2O, which began to exothermically decompose. As the N2O decomposed it released additional heat into the catpack chambers. The catpack temperatures quickly rose through 820°C when the full flow of gaseous N2O was applied through the catpacks; immediately, the engine ignited. This particular experiment demonstrated that N2O operations do not have to rely on pyrotechnic type initiators, a small amount of power to heat the catalyst packs would provide a reusable ignition technique.

5. DISCUSSION

Gaseous O2 / PMMA Performance

Combustion efficiency has proven to be extremely promising within the VFP configuration. The superb combustion efficiency is attributed to two effects directly related to the vortex action within the VFP. First, the vortex action promotes mixing of the fuel and oxidiser within the combustion chamber. Secondly, the centripetal force of the rotating gas acts to push denser (un-combusted) species toward the combustion chamber wall (away from the nozzle), re-circulating any unburned fuel and oxidiser.

Although Isp figures were deemed to be reasonable, they were not indicative of the ultimate performance of this technology; Accurate Isp measurements are difficult to achieve in a low cost R&D program. By design, emphasis was placed on performance measurement upstream of the rocket nozzle (characteristic exhaust velocity), and these measurements prove the VFP is a high performance design.

Fuel Utilisation

Of the five parameters tested for their effect on fuel mass flow rate, only geometry failed to affect the rate at which fuel was vaporised from solid form. Injection velocity, the number of injectors, combustion chamber pressure and oxidiser mass flow rate all exhibited effects on fuel mass flow rate. The fact that four input parameters play a role in fuel liberation is promising in that it indicates these parameters can be used as design tools for tailoring engine performance. The vortex patterning effect plays an important role in fuel liberation; Conventional hybrids exhibit an increasing O/F trend during operation, the VFP exhibits a decreasing O/F trend due to the vortex patterning effect. While any shift in O/F is not desirable, the decreasing O/F shift of the VFP leaves many potential remedies for "shiftless" operations (see "future research").

Since chamber geometry did not effect fuel liberation the "regression rate" of the VFP is primarily dependant on the rate at which the "Vortex Patterning" grows. Other parameters (especially injection velocity and number of injectors) affect the rate at which the patterning enhances.

Chamber Pressure Mapping

The stability and uniformity of combustion chamber pressure was astonishing within both VFP engineering models. Stable combustion chamber pressure is defined as having pressure fluctuations of les than 5% of mean; The VFP has demonstrated less than 1% pressure variations for the vast majority of the test firings. Stable combustion chamber pressure has proven to demonstrate more uniform rocket engine operations, better cooling effects and less vibration, the VFP appears to possess all of the attributes.

Engine Scalability

The engine scalability measurements demonstrated that engine scales and performs well over the regimes tested. The near-linear relationship between fuel liberation and burn surface area promises that the engine diameter could be pushed smaller or larger than the regimes tested without undue fear of adversely affecting performance. However, as the engine radius increases, the fuel area drastically increases, as fuel area increases so does the O2 mass flow rate to maintain stoichiometric operation. The end result is a direct relationship between engine diameter and thrust.

Flight Propellants

Nitrous oxide testing was promising in that stable combustion was achieved with both gaseous and liquid N2O. However, the boil-off rate of the liquid N2O was not sufficient to support the mass flow requirements of either engineering model, and liquid injection proved dangerous without significantly re-engineering a new demonstration engine. N2O does possess many positive attributes for small spacecraft propulsion therefore the author recommends that further research concentrate on "positive" ignition devices (capable of ensuring the whole fuel grain is ignited) and smaller engines that can be supplied by N2O tank boil-off.

In addition to the combustion tests performed with N2O, a novel ignition method was successfully demonstrated with gaseous N2O. In this test, EM1 was used with shell 405 packed into two catalyst packs, the catalyst packs were externally heated and N2O was passed through them. The resulting catalytic decomposition of the N2O produced enough heat to spontaneously ignite the rocket engine.

HTP operations have demonstrated exciting results (figure 23). Ignition times as low as 0.2 seconds have been demonstrated as well as extremely smooth combustion. Combustion efficiency and Isp efficiency have been very high. With HTP operations, the desire to increase the number of injectors has to weighed against the number of catalyst packs. In order to minimise the amount of heat lost to the injector assembly (and minimise ignition delay), it is recommended that each injector have its own catalyst pack.

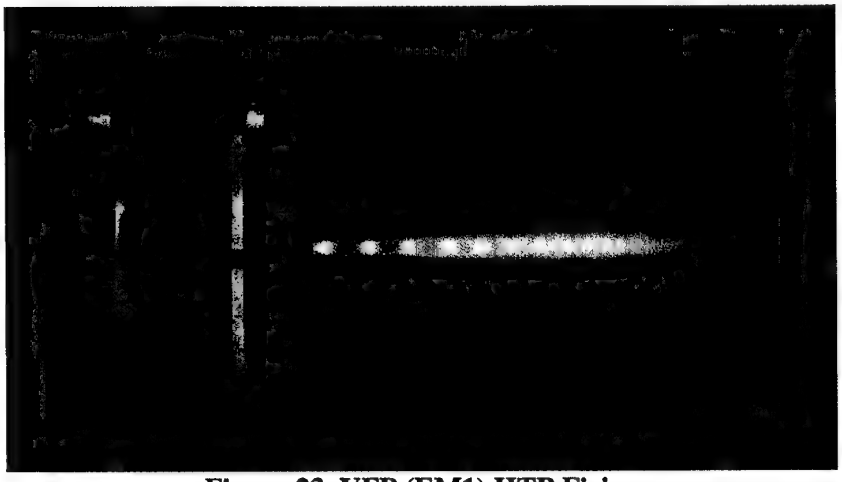

Figure 23. VFP (EM1) HTP Firing

6. PROTOTYPE DESIGN

Based upon the knowledge gathered during the VFP research program, a prototype engine is proposed. This engine utilises Degussa (89%) HTP and PE as propellants. Targeted to provide a 100m/s change in velocity on a 100kg spacecraft, the engine would contain 0.4kg of Black PE and require 2.9kg of 89% HTP (divided into eight externally mounted catalyst packs and fed tangentially into the combustion chamber).

Each catalyst pack would include a cavitating venturi at the inlet to prevent catalyst pack washout and provide an even distribution of the HTP to each of the eight catalyst packs. Each pack would consist of a stack of 100 silver gauze disks (6.9mm in diameter) pushed into a 6.9mm dia tube until the pack is 25mm long. This would result in a catpack loading factor of 100 kg/m^2 s.

Overall combustion chamber (inside) dimensions are 7cm tall by 10cm diameter. The combustion chamber would be fabricated of stainless steel. The nozzle would require a refractory metal such as Columbium with a silicon ion (anti-oxidation) coating to withstand the severe heat of the combustion products. With a 100:1 expansion ratio, the engine would provide approximately 300 seconds of vacuum Isp. With an HTP feed rate of approximately 30g/s and an average fuel mass flow rate of 3.7g/s, the engine would provide 100N of thrust (average). Figures 24, 25 illustrate the configuration.

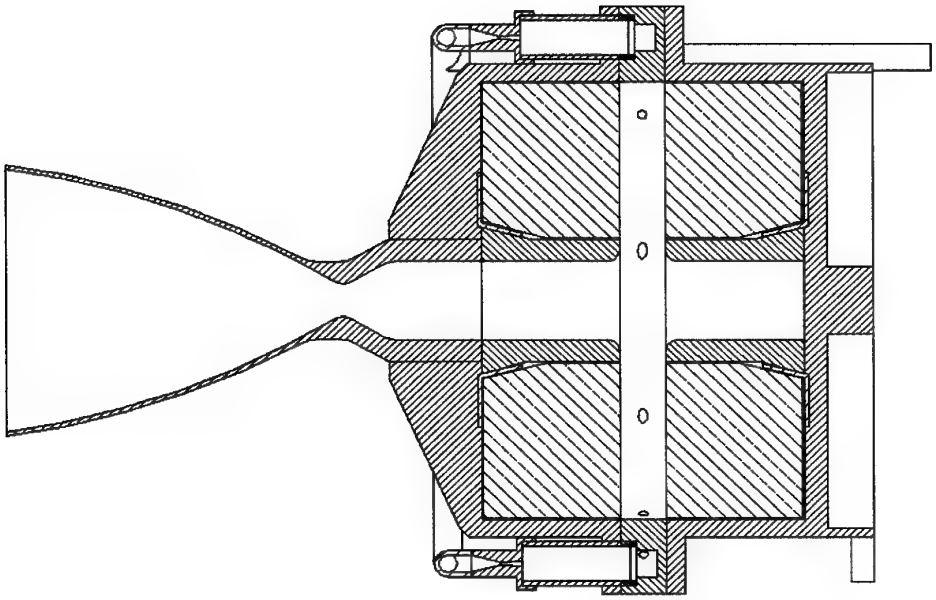

Figure 24. Cutaway view of 100N VFP Hybrid Engine

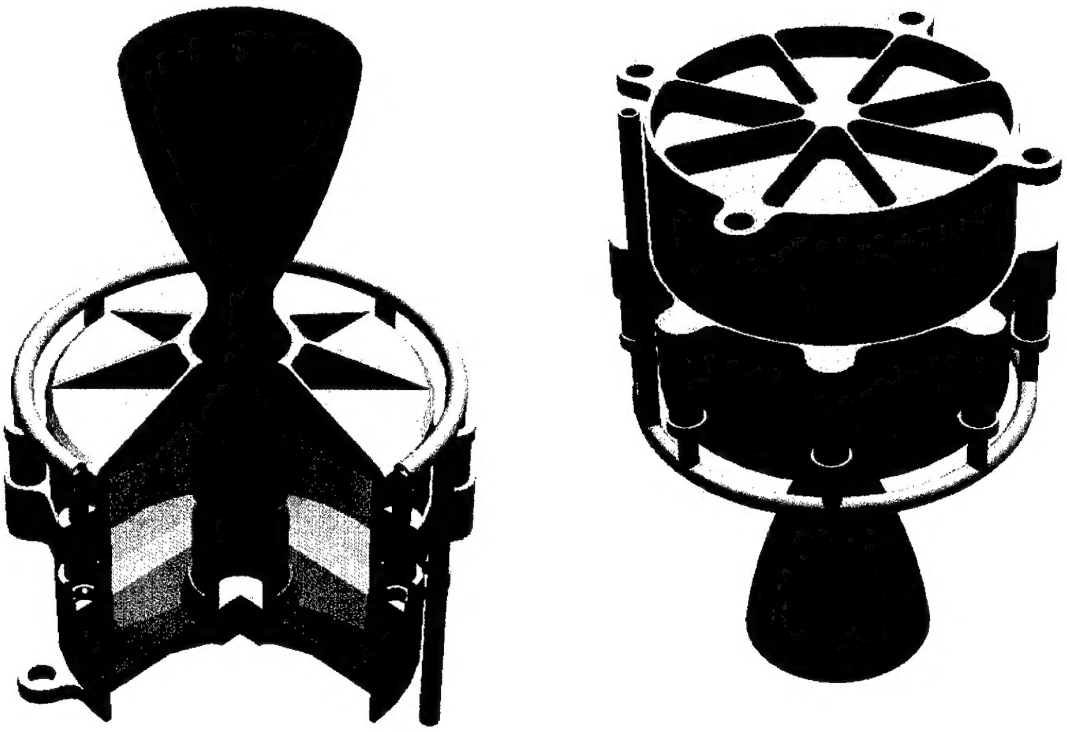

Figure 25. 100N VFP Utilising HTP and PE

7. FURTHER RESEARCH

Although the VFP engine can be employed as previously suggested, other refinements and research can be conducted to optimise the design. One particularly useful research tool providing valuable insight into the engines operation would be CFD modelling of the vortex flow field and solid fuel interface; By understanding this interaction one could possibly tailor the injection scheme or profile the fuel grains to eliminate the vortex patterning effect and subsequent increase in fuel mass flow rate. Optimisation of the existing boundary layer step configuration (overall diameter, thickness, alternative materials, etc.) has been left to follow-on research. Another area to investigate would be scaling down the engine diameter or looking into alternative fuel and oxidizer combinations that would reduce engine thrust yet still allow optimal mixing ratios. Alternatively, one could investigate adding additional boundary layer steps (radially) into the fuel grains to decrease the available fuel burn surface area within the combustion chamber or investigate a single fuel grain design (figure 26).

Nitrous oxide remains an attractive oxidiser for small spacecraft propulsion. Future research would be well advised to revisit operation of the VFP with this propellant.

The VFP engine was originally envisioned to be part of a multifunctional separation system. The configuration would leverage mass, position and strength from the single use separation system. Although the engine is ideally suited for incorporation into a separation system, the effort associated with design and qualification of multifunctional subsystem was deemed outside the scope and resources of the current research program. Future development of this technology should pursue this avenue.

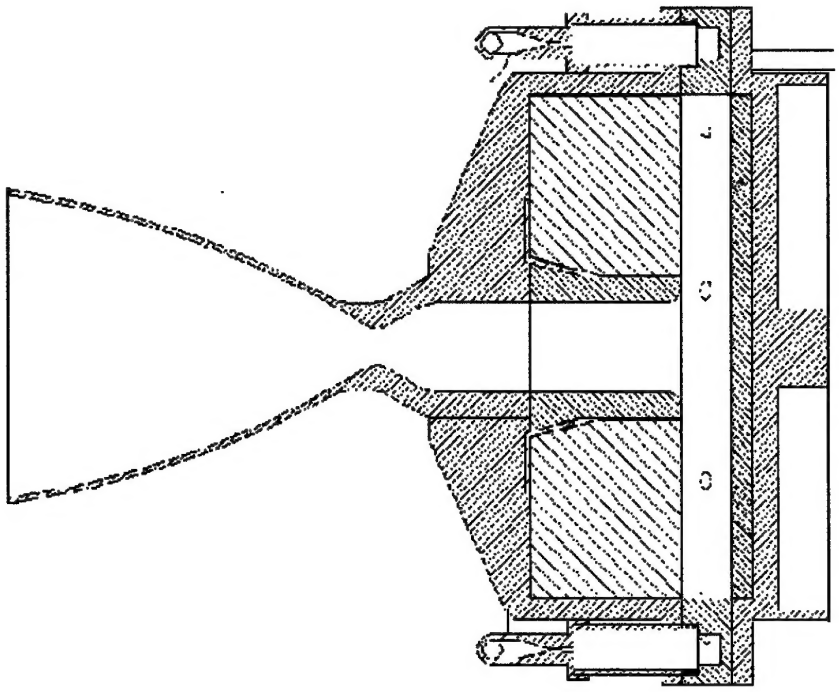

Figure 26. Cutaway View of a single grain (low thrust) VFP

7.1 Flight qualification

The engine development has now reached the stage where it can be targeted towards a flight qualification unit (based upon the design in section 6). The following work would be required to bring the engine to flight standard:

-Define performance requirements based upon a market survey of all potential applications. This would also identify flight oxidiser type.
-Build and test a number of prototype units at representative duty cycles (performed at ambient conditions).
-Build and test a number of flight weight, welded units (performed at ambient conditions).
-Build and test 2 or 3 qualification models to be test fired within a vacuum chamber (note: No vacuum test facility currently exists within the UK for this size engine)

Provided 89% HTP is selected as a flight oxidiser, parallel research would be required to develop a flight storage tank and expulsion system. Currently, SSC has commenced work on HTP compatible tanks and expulsion systems.

8. CONCLUSIONS

Although VFP testing was conducted in a low cost environment, the research program collected a wealth of valuable data with regard to this all-new hybrid rocket engine. First, it has been determined that the combustion efficiency is outstanding within the VFP. Combustion efficiencies very near 100% indicate the fuel and oxidiser mix and combust more completely than conventional designs. Although the thrust measurement infrastructure was not as robust as one would like, one must look at the results achieved in the context of a low-cost, proof-of-concept research program; accordingly, achieving Isp measurements comfortably in excess of 90% (of theoretical values) provides proof that the new rocket engine concept indeed delivers high performance.

The fuel utilisation analysis identified several parameters affecting the solid fuel liberation within the new rocket design; in addition, mathematical relationships were developed in order to aid in the design of VFP engine. The scalability test has demonstrated that the VFP indeed scales well, providing high performance over the regimes tested as well as reliable, predictable, fuel liberation based upon the engine radius. Although the VFP does exhibit an O/F shift (downward) over consecutive runs, the shift is not as drastic as the conventional hybrid O/F shift (upward) reported in the literature; in addition, it appears that the O/F shift can be minimised or possibly eliminated through a combination of low injection velocity and multiple injectors.

The chamber pressure mapping did not reveal any pressure gradient across the diameter of the VFP rocket engine over the regimes tested. While a pressure gradient is observed during cold flow and engine start-up, the gradient quickly vanishes as full combustion is achieved. Although there still appears to be an enhanced fuel and oxidiser mixing effect, it is hypothesised that the solid fuel boundary layers are significantly impeding the free flow vortex within the VFP combustion chamber which has the positive effect of reducing the probability of exhaust wastefully spinning out the exhaust nozzle.

Flight propellant testing was promising in a number of areas. First, the VFP demonstrated high performance operations with HTP and PE; both combustion efficiency and Isp figures averaged approximately 95%. Testing with N2O uncovered VFP regimes that can result in a high pressure excursion; although completely avoidable by measures outlined, the VFP can pool liquid oxidiser and must be tested with this characteristic in mind. N2O operations are entirely plausible within the VFP and the novel method discovered for igniting a N2O hybrid further support it's development (at flow levels supportable by the N2O vapour pressure).

The VFP has demonstrated the ability to operate smoothly for long durations (up to 45 seconds tested), and return to within 1.5% of operational values upon relight (pulsed operations). The inherent gas separation and film cooling indicate that the VFP combustion chamber can be constructed of common (inexpensive) construction materials. In addition to having a higher volumetric loading factor than conventional hybrid designs, the centripetal force within the combustion chamber has demonstrated a tendency to keep the nozzle clear from solid particulate, this feature promises that the engine may be burned near completion without the fear of solid fuel slivers blocking the rocket nozzle.

The VFP test campaign provides solid evidence that the VFP is superior to conventional hybrid design in almost every respect and holds great promise for small spacecraft applications. Additional supporting material can be found in [Haag 01].

The research program has reached the point where research can be continued (as outlined in paragraph 7.0) or steps can be taken towards flight qualification (paragraph 7.1). SSTL is currently in the process of identifying in house missions and external customers to demonstrate this technology. Currently, the ESA SSETI programme is demonstrating interest in the engine. Finally, as orbital debris mitigation comes closer to reality, SSTL realises that future legislation may require a low cost yet robust capability to de-orbit spacecraft, the VFP technology stands ready to assist this requirement.

Bibliography

[Goldman 96] Goldman, C., Gany, A., "*Thrust Modulation of Ram Rockets by a Vortex Valve*", Technion- Israel Institute of Technology, Israel, AIAA 96-2624.

[Haag 01] Haag, G., S., "*Alternative Geometry Hybrid Rockets For Spacecraft Orbit Transfer*", Ph.D. Dissertation, University of Surrey, September 2001.

[Humble 95] Humble, R., Henry, G., Larson, W., *Space Propulsion Analysis and Design-Revised*, McGraw-Hill, New York, NY, 1995.

[McCormick 65] McCormick, J., "*Hydrogen Peroxide Rocket Manual*", FMC Corporation, 1965

[Selph 92] Selph, C., Isp Computational Computer Code, AFRL, 1992.

[Sutton 92] Sutton, G., *Rocket Propulsion Elements*, 6th ed., John Wiley and Sons, New York, NY, 1992.

[UoH 00] University of Houston website: www.ifdt.uh.edu/vtc/rotate.html

[Zakirov 00] Zakirov, V.A., T.J. Lawrence, J.J. Sellers, and M.N. Sweeting, *"Nitrous Oxide as a Rocket Propellant*", Proceedings of the 51st International Astronautical Federation Congress, Rio de Janeiro, Brazil, 2-6 October 2000.

[Zakirov 01] Zakirov, V.A., T.J. Lawrence, and M.N. Sweeting, *"An Update on Surrey Nitrous Oxide Catalytic Decomposition Research"*, Proceedings of the 15th Annual AIAA/USU Conference on Small Satellites, the United States, 13-16 August 2001.